Structure of the unusual *Sinorhizobium fredii* HH103 lipopolysaccharide and its role in symbiosis

Received for publication, March 10, 2020, and in revised form, June 11, 2020 Published, Papers in Press, June 16, 2020, DOI 10.1074/jbc.RA120.013393

Flaviana Di Lorenzo[1], Immacolata Speciale[1], Alba Silipo[1], Cynthia Alías-Villegas[2], Sebastián Acosta-Jurado[2], Miguel-Ángel Rodríguez-Carvajal[3], Marta S. Dardanelli[4], Angelo Palmigiano[5], Domenico Garozzo[5], José-Enrique Ruiz-Sainz[2], Antonio Molinaro[1,*], and José-María Vinardell[2,*]

From the [1]Department of Chemical Sciences, University of Naples Federico II, Napoli, Italy, [2]Department of Microbiology, Faculty of Biology, University of Seville, Sevilla, Spain, [3]Deparment of Organic Chemistry, Faculty of Chemistry, University of Seville, Sevilla, Spain, [4]Departamento de Biología Molecular, Facultad de Ciencias Exactas, Físico-Químicas y Naturales, Universidad Nacional de Río Cuarto-INBIAS, CONICET, Córdoba, Argentina, and [5]Istituto per i Polimeri, Compositi e Biomateriali IPCB, Consiglio Nazionale delle Ricerche, Catania, Italy

Edited by Chris Whitfield

Rhizobia are soil bacteria that form important symbiotic associations with legumes, and rhizobial surface polysaccharides, such as K-antigen polysaccharide (KPS) and lipopolysaccharide (LPS), might be important for symbiosis. Previously, we obtained a mutant of *Sinorhizobium fredii* HH103, *rkpA*, that does not produce KPS, a homopolysaccharide of a pseudaminic acid derivative, but whose LPS electrophoretic profile was indistinguishable from that of the WT strain. We also previously demonstrated that the HH103 *rkpLMNOPQ* operon is responsible for 5-acetamido-3,5,7,9-tetradeoxy-7-(3-hydroxybutyramido)-L-*glycero*-L-*manno*-nonulosonic acid [Pse5NAc7(3OHBu)] production and is involved in HH103 KPS and LPS biosynthesis and that an HH103 *rkpM* mutant cannot produce KPS and displays an altered LPS structure. Here, we analyzed the LPS structure of HH103 *rkpA*, focusing on the carbohydrate portion, and found that it contains a highly heterogeneous lipid A and a peculiar core oligosaccharide composed of an unusually high number of hexuronic acids containing β-configured Pse5NAc7(3OHBu). This pseudaminic acid derivative, in its α-configuration, was the only structural component of the *S. fredii* HH103 KPS and, to the best of our knowledge, has never been reported from any other rhizobial LPS. We also show that Pse5NAc7(3OHBu) is the complete or partial epitope for a mAb, NB6-228.22, that can recognize the HH103 LPS, but not those of most of the *S. fredii* strains tested here. We also show that the LPS from HH103 *rkpM* is identical to that of HH103 *rkpA* but devoid of any Pse5NAc7(3OHBu) residues. Notably, this *rkpM* mutant was severely impaired in symbiosis with its host, *Macroptilium atropurpureum*.

Rhizobia are soil bacteria able to establish a symbiotic association with legumes in which a complex interchange of molecular signals between the prokaryotic and the eukaryotic partners takes place. This interchange of molecular signals culminates in the formation of specialized plant structures, called nodules, on the roots or stems of the plant host (1). The molecular dialogue between the bacteria and the plant is initiated by flavonoids exuded by the legume root, which activate the transcription of bacterial nodulation genes. Some of these genes encode proteins involved in the biosynthesis and secretion of molecular signals called Nod factors. These bacterial signals mediate species specificity and induce the development of root nodules in the plant (1–3).

In addition to Nod factors, different rhizobial surface polysaccharides (RSP) are commonly necessary for successful nodulation. Exopolysaccharides (EPS), lipopolysaccharides (LPS), capsular polysaccharides (KPS or K-antigen polysaccharides), and cyclic glucans (CG) are the main rhizobial polysaccharides involved in symbiosis. For each specific pair of rhizobium-legume symbionts, one or more RSP could act as signal molecules promoting bacterial infection and/or preventing plant defense reactions (4–7).

Sinorhizobium fredii HH103 (8) is a fast-growing rhizobial strain that nodulates *Glycine max* (soybean) and many other determinate- and indeterminate-nodule forming legumes (9). This bacterium produces at least five different RSP: EPS, LPS, CG, and two types of KPS. The chemical structure of these RSP, except for the LPS, have been previously described (10–13). Interestingly, two KPS are produced by *S. fredii* HH103, one is a homopolysaccharide built up of a pseudaminic acid derivative, *i.e.* α-configured 5-acetamido-3,5,7,9-tetradeoxy-7-(3-hydroxybutyramido)-L-*glycero*-L-*manno*-nonulosonic acid [α-Pse5NAc7(3OHBu)] (12), whereas the other is a homopolymer of 3-deoxy-D-*manno*-oct-2-ulosonic acid (Kdo) (13). To our knowledge, *S. fredii* HH103 mutants affected in the production of the poly-Kdo KPS have not been described. An *S. fredii* Rif^R *exoA* mutant, unable to produce EPS, did not show any detectable reduction in the symbiotic capacity with soybean (10). On the contrary, soybean plants inoculated with HH103 mutants unable to produce CG only formed pseudonodules that did not fix nitrogen (11). Interestingly, *S. fredii* HH103 Rif^R mutants in genes located in the so-called *rkp-1* region (such as HH103 *rkpA*) showed a severe reduction of nodulation with soybeans (14–16). HH103 *rkpA* failed to produce the poly-α-Pse5NAc7(3OHBu) KPS, but the other RSP did not show any detectable change. Even more importantly, *S. fredii* HH103 Rif^R mutants in genes located in the so-called *rkp-3* region (such as *rkpM*, *rkpP*, or *rkpQ*) did not produce the α-Pse5NAc7(3OHBu) KPS as well, showed altered LPS electrophoretic

This article contains supporting information.

* For correspondence: José-María Vinardell, jvinar@us.es; Antonio Molinaro, molinaro@unina.it.

Table 1
Previously studied *Sinorhizobium fredii* HH103 mutants affected in LPS

Mutated gene	Predicted function of the encoded product	RSP affected[a]	Symbiotic phenotype with soybean	Reference
lpsB	Glycosyl transferase	LPS*	High reduction in the number of Fix^+ nodules, pseudonodules	31
lpsE	Glycosyl transferase	LPS*		
lpsL	UDP-glucuronate 4-epimerase	LPS*	Pseudonodules, Fix^-	37
rkpK	UDP-glucose 6-dehydrogenase	LPS* EPS^-	Nod^+ Fix^+ (as WT)	
rkpM	Pyridoxal phosphate (PLP)-dependent aminotransferase	LPS* KPS^-	Pseudonodules, Fix^-	17

[a] LPS* refers to alterations in the electrophoretic profile and lack of recognition by the mAb NB6-228.22.

profiles, and only induced the formation of soybean pseudonodules unable to fix nitrogen (17).

LPS are the predominant constituents in the external leaflet of Gram-negative outer membrane and can be conceptually divided in three different structural regions: a glycolipid component called lipid A that is linked to a core oligosaccharide (core OS) that is attached to an outer polysaccharide, termed the O-chain (18). On the basis of the nature of the saccharide portion, an LPS can be classified as smooth, semirough, or rough: smooth-type LPS (S-LPS) contains all three abovementioned domains, whereas a semirough-type LPS (sR-LPS) has a subunit (complete or truncated) of the O-chain, and a rough-type LPS (R-LPS) does not express any O-chain moiety (18).

To the best of our knowledge, the complete LPS structure has only been described for five different rhizobial strains: *Rhizobium etli* CE3, *R. leguminosarum* biovar *viciae* 3841, *R. leguminosarum* biovar *viciae* 128C53 (19), and *Bradyrhizobium* sp. strain BTAi1 and ORS285 (20–22); in addition, only partial structures or the chemical composition of different LPS parts of various *Sinorhizobium* strains have been reported (23). Nevertheless, it is widely known that rhizobial LPSs appear to play very relevant roles at different stages of the symbiotic interaction with legumes, including recognition and infection, invasion of root cortical cells, bacterial penetration into nodule cells, and formation and persistence of functional symbiosomes (1, 19, 24–31). Indeed, it has been demonstrated that alterations in the LPS structure can potently affect the symbiotic properties of the bacterium; in particular, O-chain rhizobial mutants were reported to be drastically affected in symbiosis, either in the infection event, nodule development, or bacteroid differentiation, and this phenomenon has been observed with both determinate and indeterminate nodule-forming legumes (32–36).

In this work, we focused attention on the LPS isolated from two *S. fredii* HH103 Rif^R mutants: HH103 *rkpA* (16) and HH103 *rkpM* (17). HH103 *rkpA* was chosen because it does not produce KPS, which could interfere with LPS purification, and its LPS silver- and immune-staining profiles were equal to those of *S. fredii* HH103 Rif^R, indicating that the LPS structure of both strains should be highly similar or identical. In parallel, HH103 *rkpM* was investigated because it does not produce KPS as well, and its LPS silver-staining profile was shown to be only slightly altered with respect to *S. fredii* HH103 Rif^R. Structural investigation showed that HH103 *rkpA* possesses an LPS containing β-Pse5NAc7(3OHBu), which was never described before as a component of this polysaccharide in rhizobia. Interestingly, we also show that *S. fredii* HH103 *rkpM* produces an LPS devoid of such pseudaminic acid derivatives, and that this mutant is severely impaired in symbiosis with the HH103 host legume *Macroptilium atropurpureum*.

Results

Silver staining and antibody recognition of the LPS produced by different S. fredii HH103 mutants affected in LPS and/or KPS biosynthesis

In previous works (17, 31, 37), we have studied different *S. fredii* HH103 mutants (in the *rkpM*, *lpsB*, *lpsE*, *rkpK*, and *lpsL* genes) that were affected in LPS production, as revealed by alterations in their LPS electrophoretic profiles. Relevant characteristics of these mutants are summarized in Table 1. The *lpsB* and *lpsE* genes belong to the *greA lpsB lpsCDE* cluster and are predicted to code for type 1 glycosyltransferases that transfer activated sugars to a variety of substrates, including glycogen and LPS (31). The *rkpK* and *lpsL* genes constitute the so-called *rkp-2* region, and their encoded products are responsible for the synthesis of glucuronic and galacturonic acid, respectively (37). Finally, the *rkpM* gene belongs to the *rkpLMNOPQ* operon (*rkp-3* region), which is involved in the production of the pseudaminic acid derivative that constitutes the HH103 KPS (17). In this work, we have compared their LPS profiles in a single polyacrylamide gel (Fig. 1*A*) to classify them according to the mobility of the silver-stained LPS bands. We hypothesized that any increase of the electrophoretic mobility of the LPS bands would be directly related to the size of the truncated LPS forms produced by each mutant. Therefore, mutants showing faster migrating LPS bands might correspond to mutants producing smaller truncated LPS core OS forms. WT *S. fredii* HH103 Rif^R and its *rkpA* mutant derivative were also included as controls, because this mutant does not produce KPS but its LPS shows the same electrophoretic profile of HH103 Rif^R (16).

Figure 1*A* allowed us to compare the electrophoretic alterations exhibited by the different mutants. As shown in this figure, the LPS profile of *S. fredii* HH103 Rif^R is composed of four silver-stained bands of slower mobility and two thick bands of faster mobility. This observation suggested that bands in the upper part of the gel would correspond to LPS molecules made up of lipid A, core OS, and O-chain (or part of it), whereas in the lower part of the gel a smaller LPS, migrating as a dispersed thick region, was assumed to contain the lipid A and core OS with no O-chain subunits. The biological nature of the tiny smears visualized in the upper part of the gel remains unknown. At the bottom of each lane appears a diffuse band that is not always visualized in SDS-PAGE gels carried out with HH103 LPS samples (16, 17) and whose nature is unknown.

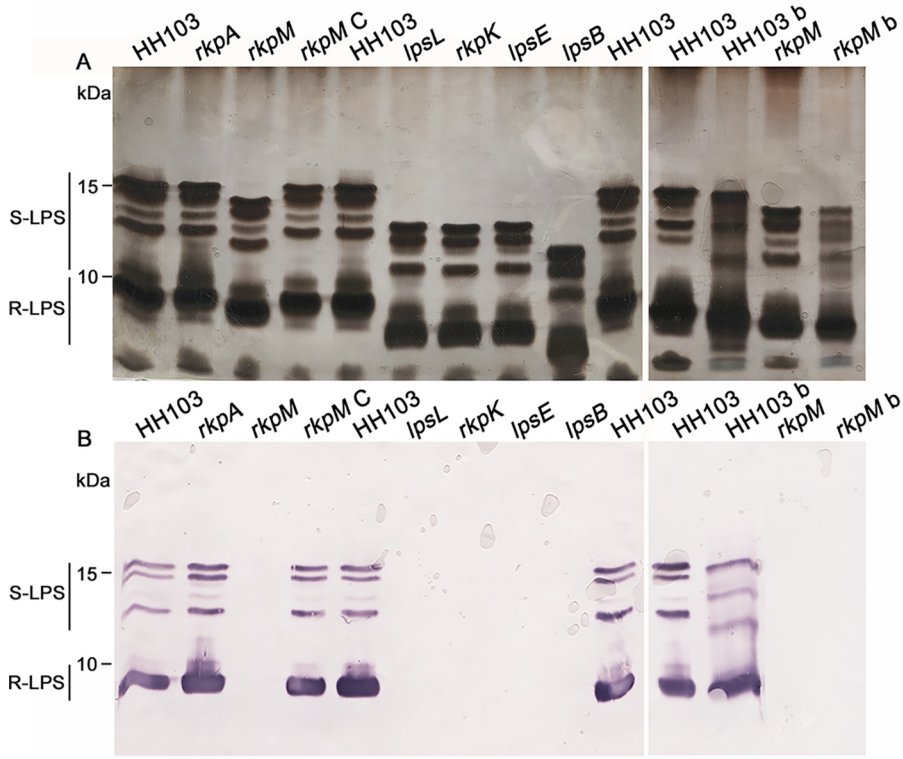

Figure 1. Electrophoretic profile and immunodetection of the LPS produced by different *S. fredii* HH103 Rif^R mutants affected in LPS and/or KPS production. *A*, SDS-PAGE after silver staining of LPS crude extracts. *B*, immunostaining using the mAb NB6-228.22 of LPS crude extracts. In both *panels A* and *B*, the mutated gene is indicated on the top of the lane. HH103 denotes HH103 Rif^R, and *rkpM* C denotes the complemented *rkpM* mutant. All of the samples were extracted from free-living cells, with the only exception being samples HH103 b and *rkpM* b, which correspond to samples extracted from bacteroids from *Glycyrrhiza uralensis* nodules induced by HH103 Rif^R and its *rkpM* mutant, respectively.

As reported before (17, 31, 37), the electrophoretic mobility of the bands of the five HH103 mutants affected in LPS was clearly faster than that of HH103 Rif^R or its *rkpA* derivative. However, there were also differences among the different LPS mutants (Fig. 1*A*): mutants in *lpsL*, *rkpK*, and *lpsE* showed similar LPS profiles with faster electrophoretic mobility than that of HH103 *rkpM* but slower than that of HH103 *lpsB*.

Following these observations, we employed NB6-228.22, a mAb able to recognize all the silver-stained LPS bands of *S. fredii* HH103 Rif^R (38). As shown in Fig. 1*B*, the pattern of LPS bands recognized by NB6-228.22 in *S. fredii* HH103 Rif^R was equal to that in HH103 *rkpA*. Neither the tiny smears at the upper part nor the diffuse bands at the bottom of the gels reacted with the antibody. None of the *S. fredii* HH103 Rif^R mutants showing alterations in their LPS electrophoretic profiles (*rkpM*, *lpsL*, *rkpK*, *lpsE*, and *lpsB*) were recognized by NB6-228.22, indicating that in all these mutants the LPS epitope recognized by NB6-228.22 was missing or has become unavailable for antibody recognition. Introduction in HH103 *rkpM* of a cosmid containing the HH103 *rkp-3* region (strain HH103 *rkpM* C) restored the WT LPS profile (Fig. 1*A*) and recognition by the mAb NB6-228.22 (Fig. 1*B*).

LPS profiles of *S. fredii* HH103 Rif^R free-living cells is undistinguishable from HH103 Rif^R bacteroids isolated from *G. max* or *C. cajan* (39). However, *S. fredii* HH103 Rif^R bacteroids isolated from *Glycyrrhiza uralensis* showed altered LPS profiles compared with those of *S. fredii* HH103 free-living cells (39). Given these premises, the LPS from bacteroids of *G. uralensis* nodules induced by inoculation with HH103 Rif^R or HH103 *rkpM* were also analyzed by SDS-PAGE in the present study (Fig. 1*A*). The LPS profile of HH103 *rkpM* bacteroids was slightly different from that of free-living HH103 *rkpM* cells and clearly altered with respect to that of HH103 bacteroids. This demonstrated that HH103 *rkpM* LPS is altered not only in free-living cells but also in *G. uralensis* bacteroids compared with those of the WT strain. The LPS of HH103 *rkpM* bacteroids isolated from *Glycyrrhiza* nodules was not recognized by the mAb NB6-228.22 (Fig. 1*B*).

Taking into account all the above results, we started the structural characterization of the LPS of HH103 mutants *rkpA* and *rkpM*.

Structural determination of the LPS from S. fredii HH103 rkpA and HH103 rkpM mutants

To define the detailed structure of *S. fredii* HH103 *rkpA* and HH103 *rkpM* LPS, the dried bacterial pellets were extracted by the hot phenol-water procedure (40), checked by SDS-PAGE, and extensively purified. To define the nature of the monosaccharides composing the isolated LPSs, a set of chemical analyses (41) on pure water phase extracts was performed. The merging of data from compositional analysis, through acetylated methyl glycosides derivatization, and absolute configuration, through octyl glycoside derivatization, revealed the presence in both LPS of D-galacturonic (D-GalA) and D-glucuronic

(D-GlcA) acids, D-glucose (D-Glc), D-galactose (D-Gal), 2-amino-2-deoxy-D-glucose (D-GlcN), and Kdo. Linkage analyses (41) proved the pyranose form for all sugar residues and allowed the identification of the same branching points for the monosaccharides composing both the LPS, except for terminal-D-Gal*p*A, which was found only in the case of HH103 *rkpM*, and 2-substituted-D-Gal*p*A, which was found instead only in the case of HH103 *rkpA*; on the other hand, 4-substituted D-Gal*p*A, terminal and 2-substituted D-Glc*p*A, 2-substituted and 3-substituted D-Glc*p*, 3,6-disubstituted D-Gal*p*, 6-substituted-D-Glc*p*N, and terminal and 4,5-disubstituted Kdo were detected in both LPS. Importantly, as described further in the text, an additional sugar constituent, Pse5NAc7(3OHBu) (Pse), was identified solely in HH103 *rkpA* and only after an in-depth investigation of the isolated LPS saccharide component using NMR spectroscopy and MALDI-TOF MS.

To define the primary structure of the saccharide portion of both HH103 *rkpA* and HH103 *rkpM* LPS, an aliquot of each sample underwent a mild acid hydrolysis to selectively cleave the linkage between the Kdo, which is the first sugar component of the core OS, and the lipid A moiety. After several steps of purification comprising size-exclusion low-pressure and HPLC, the pure saccharide moieties (**OS1**$_{rkpA}$ and **OS1**$_{rkpM}$) were analyzed via 1D and 2D NMR spectroscopy, including double-quantum filtered phase-sensitive correlation spectroscopy (DQF-COSY), total correlation spectroscopy (TOCSY), rotating frame Overhauser enhancement spectroscopy (ROESY), heteronuclear single quantum coherence (^{1}H-^{13}C HSQC), ^{1}H-^{13}C HSQC-TOCSY, and heteronuclear multiple bound correlation (^{1}H-^{13}C HMBC).

All sugar units were present as pyranose rings according to the ^{13}C chemical shift values and in full accordance with chemical analyses. The analysis of both the ^{1}H NMR (Fig. 2) and HSQC spectra (Fig. 3) of the pure **OS1**$_{rkpA}$ clearly showed the occurrence of eight anomeric signals attributed to eight different spin systems (**A**–**H**, Table 2), whereas the presence of a Kdo unit was attested by the presence of the diasterotopic H-3 methylene proton signals at δ_H 1.94/1.75 ppm (**K**, δ_C 33.9 ppm, Fig. 2 and 3). Furthermore, the ^{1}H NMR spectrum (Fig. 2) showed the presence of four intense methyl signals at δ_H 1.05, 1.09, 1.11, and 1.13 ppm (Table 2) and of another intense methyl signal at 1.90 ppm accounting for two *N*-acetyl groups (*N*Ac). Finally, the presence of additional methylene proton signals at 1.55/2.42 ppm (**Pse^{I}** H-3$_{ax}$/H-3$_{eq}$, δ_C 36.0 ppm) and 1.50/2.47 ppm (**Pse^{II}** H-3$_{ax}$/H-3$_{eq}$, δ_C 36.1 ppm) were also identified. Starting from the above methylene signals, the analysis of HSQC and HMBC spectra, supported by the correlations visible in COSY, TOCSY, and ROESY spectra, allowed the complete structural elucidation of two Pse residues (here indicated as **Pse^{I}** and **Pse^{II}**). Briefly, the diasterotopic methylene protons H-3 **Pse^{I}** showed long-range correlations with an oxymethine carbon atom (C-4 **Pse^{I}**, δ_C 66.3 ppm), a quaternary carbon (C-2 **Pse^{I}**, δ_C 103.2 ppm), and a carboxylic group (C-1 **Pse^{I}**, δ_C 172.8 ppm) (Fig. 4). A less intense HMBC correlation between H-3$_{ax}$ **Pse^{I}** and a nitrogen-bearing carbon atom resonating at 48.0 ppm (C-5 **Pse^{I}**) was also detected (Fig. 4) and identified as the site of *N*-acetylation, as proven by the NOE correlation between H-5 **Pse^{I}** (4.05 ppm) and the methyl proton at 1.90 ppm (not shown). Starting from H-5 **Pse^{I}**, a long-range correlation with an oxymethine carbon atom at 73.0 ppm, assigned as C-6 **Pse^{I}**, was visible in the HMBC spectrum (Fig. 4); further on, the methyl proton signal at 1.09 ppm correlated with an oxymethine carbon atom (C-8 **Pse^{I}**, 68.3 ppm) and a nitrogen-bearing carbon (C-7 **Pse^{I}**, 53.7 ppm), with the latter, in turn, correlated to H-6 **Pse^{I}** (3.77 ppm) (Fig. 4). Finally, a 3-hydroxybutyryl moiety (HBu, made up of the *C*H$_3$-C group at δ_C 22.0 ppm, the C-*C*HOH-C group at δ_C 69.8 ppm, the C-*C*H$_2$-C at δ_C 45.0 ppm, and the *C*O group at 173.4 ppm) was found to be connected by amide linkage at position 7 of **Pse^{I}**; the location of the HBu moiety was attained by the observation of a long-range correlation between *C*-1′ (173.4 ppm) and H-7 **Pse^{I}** (3.94 ppm) in the HMBC spectrum (Fig. 4). Because of the relatively large $J_{H\text{-}3ax,H\text{-}4}$ (~12.9 Hz) and the small $J_{H\text{-}4,H\text{-}5}$ and $J_{H\text{-}5,H\text{-}6}$ (<5 Hz) coupling constants, it was possible to deduce the axial orientation of H-4 **Pse^{I}** and the equatorial orientation of H-5 **Pse^{I}** that combined with the $J_{H\text{-}6,H\text{-}7}$ coupling constant of ~10 Hz, suggested the L-*glycero*-L-*manno* configuration of unit **Pse^{I}** (42). This was also corroborated by the observation of the chemical shift for the C-9 signal at 16.2 ppm (Table 2), which is typical of the L-epimer of the *glycero*-L-*manno* isomers; in contrast, chemical shifts at around 20 ppm are observed in the case of the D-epimers (42). Interestingly, the large difference between the H-3$_{ax}$ and H-3$_{eq}$ chemical shifts (0.88 ppm) indicated the axial orientation of the carboxyl group, which is the β configuration of **Pse^{I}** at the anomeric center (42). Finally, the downfield displacement of the chemical shift of C-3′ (69.8 ppm) of unit **Pse^{I}** suggested a site of glycosylation at such a position. Similarly, a second unit of β-Pse5NAc7(3OHBu) has been assigned (**Pse^{II}**), but it turned out to be a terminal residue, linked to position 3′ of **Pse^{I}**, as proven by the long-range correlation between the C-2 of **Pse^{II}** and the oxymethine proton H-3′ (4.13 ppm, Table 2 and Fig. 4) of **Pse^{I}**. The absolute configuration of the HBu substituent remains to be defined.

As for the other spin systems, **A** (H-1 at 5.53 ppm, Table 2), **B** (H-1 at 5.50 ppm), **C** (H-1 at 5.09 ppm), **F** (H-1 at 4.55 ppm), and **H** (H-1 at 4.23 ppm) were identified as hexuronic acid residues because of the correlation of their H-5 signals with carboxyl groups resonating at 175.3, 175.1, 175.5, 174.9, and 174.2 ppm, respectively. The $^{3}J_{H\text{-}3,H\text{-}4}$ and $^{3}J_{H\text{-}4,H\text{-}5}$ coupling constant values (3 and 1 Hz, respectively) measured for **A**, **B,** and **F** were diagnostic of a *galacto* configuration, whereas the large ring $^{3}J_{H,H}$ coupling constants observed for **C** and **H** led to their identification as *gluco*-configured sugar units. The α-anomeric configuration for **A**, **B**, and **C** was attributed on the basis of the intra-residual NOE contact of H-1 with H-2 and the $^{3}J_{H1,H2}$ coupling constant values, whereas the β-anomeric configuration for residues **F** and **H** was inferred by the large $^{3}J_{H\text{-}1,H\text{-}2}$ values and the NOE contacts of H-1 with H-3 and H-5. Therefore, **A** and **B** were identified as α-GalA units, **C** as an α-GlcA, **F** as a β-GalA, and **H** as a β-GlcA. Residue **D** (H-1 at 5.04 ppm, Table 2) was identified as α-Gal because of the small $^{3}J_{H,H}$ values for H-3/H-4 and H-4/H-5, whereas residues **E** (H-1 at 5.00 ppm) and **G** (H-1 at 4.26 ppm) were assigned to α- and β-Glc, respectively.

Low-field shifted carbon signals (Table 2 and Fig. 3) were useful to identify substitution at O-4 of residues **A** and **B**, at O-2 of **F** and **H**, at O-3 and O-6 of **D**, at O-3 of **G**, at O-4 and O-5

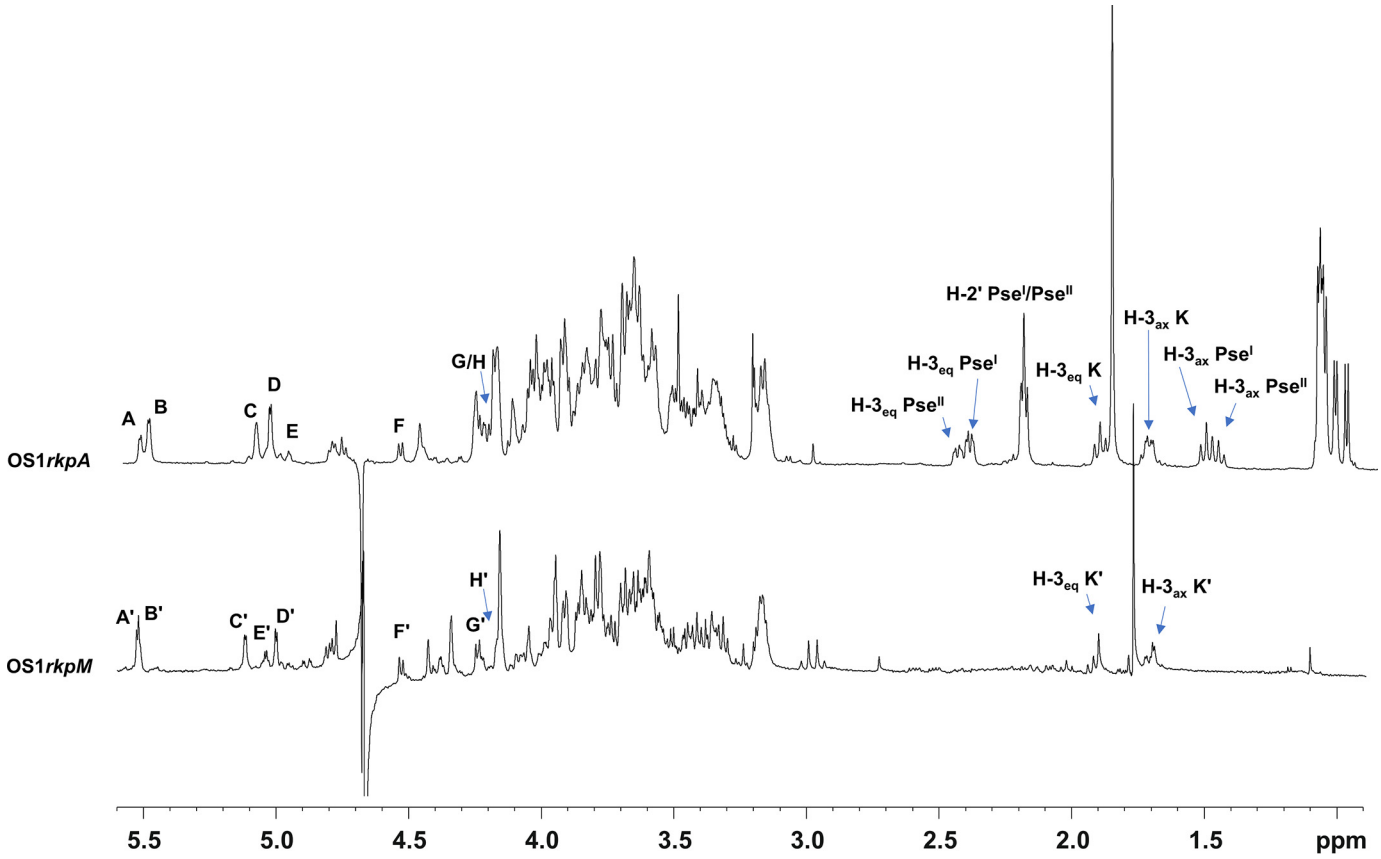

Figure 2. ^{1}**H NMR spectra of *Sinorhizobium fredii* HH103 *rkpA* (*top*) and *rkpM* (*bottom*).** Anomeric signals of spin systems are designated as described in Table 2. Diastereotopic methylene proton signals of **Pse^{I}**, **Pse^{II}**, and Kdo residues (**K**/**K'**) are also indicated.

of **K**, and, as described above, at O-3′ of **Pse^{I}**; on the other hand, residues **C**, **E**, and **Pse^{II}** were ascribed to terminal sugar units. The sequence of the monosaccharide residues was deduced by using both NOE correlations attained from the ROESY spectrum and the long-range correlations of the HMBC spectrum. In detail, the scalar interresidue long-range connections H-1 **D**/C-5 **K**, H-1 **E**/C-4 **K**, H-**1 C**/C-3 **D**, H-1 **G**/C-6 **D**, H-1 **A**/C-3 **G**, H-1 **H**/C-4 **A**, H-1 **B**/C-2 **H**, H-1 **F**/C-4 **B**, H-2 **F**/C-2 **Pse^{I},** and H-3′ **Pse^{I}**/C-2 **Pse^{II}** (Fig. 4) were identified and led to the structural assessment of the **OS1$_{rkpA}$** product (Fig. 5).

To gain further structural information about HH103 *rkpA* LPS, an aliquot of sample underwent a complete deacylation step by hydrazinolysis followed by strong alkaline treatment. This approach provides the complete oligosaccharide moiety comprising the disaccharide lipid A backbone and allows us to evaluate the presence of substituents that could have been lost during the mild acid hydrolysis procedure. Indeed, despite the great heterogeneity observed in the product because of the harsh alkaline treatment and the intrinsic nature of the oligosaccharide, the NMR analysis of the obtained product (**OS2$_{rkpA}$**) clearly disclosed, in addition to the signals relative to the α-GlcN (**X**) and β-GlcN (**Y**) of the lipid A (Table 2, Fig. S1), the occurrence of a further Kdo unit (**J**) whose methylene proton signals resonated at 1.86/2.11 ppm (δ_C 33.9 ppm). Finally, the observation of the low-field position of the signal for C-2 (75.4 ppm) of the α-Glc (**E$_2$**) linked to the 4,5-α-Kdo (**K$_2$**), and the occurrence of an NOE correlation between H-3 **J** and H-2 of **E$_2$** led to the determination of the sequence **J**-(2→2)-**E$_2$**-(1→4)-**K$_2$**, with the latter Kdo unit as the one linked to β-GlcN (**Y**) of lipid A. Therefore, summarizing all results arising from mild acid hydrolysis and full deacylation procedures, we found that HH103 *rkpA* LPS possesses a novel carbohydrate backbone made up of a disaccharide of β-Pse5NAc7(3OHBu), two Kdo units, one α-D-Glc*p*, one D-β-Glc*p*, one D-α-Gal*p*, two D-α-Gal*p*A, one D-β-Gal*p*A, one D-α-Glc*p*A and one D-β-Glc*p*A, as sketched in Fig. 5.

A similar approach was used to elucidate the structure of **OS1$_{rkpM}$** (Table S1). The comparison of the NMR spectra of **OS1$_{rkpM}$** and **OS1$_{rkpA}$** (overlapped HSQC spectra are reported in Fig. S2) revealed an identical structure apart from the absence of any Pse residue in **OS1$_{rkpM}$**. Indeed, as shown by both the ^{1}H and the HSQC NMR spectra (Fig. 2 and Fig. S2), no signals relative to the methylene and methyl groups of Pse residues were visible. Consequently, the β-GalA unit **F'** of **OS1$_{rkpM}$** (Table S1), corresponding to residue **F** in the *rkpA* mutant, was identified as a terminal sugar because of the lack of glycosylation at position O-2 by the Pse moiety. Therefore, the structure of the saccharide backbone of *rpkM* mutant LPS is as reported in Fig. 5. In the case of HH103 *rkpM*, the NMR investigation (not shown) of the fully deacylated product (**OS2$_{rkpM}$**) confirmed the occurrence of a terminal Kdo unit, lost during the mild acid hydrolysis treatment, as also proven by MALDI-TOF MS analysis executed on intact HH103 *rkpM* LPS (see below).

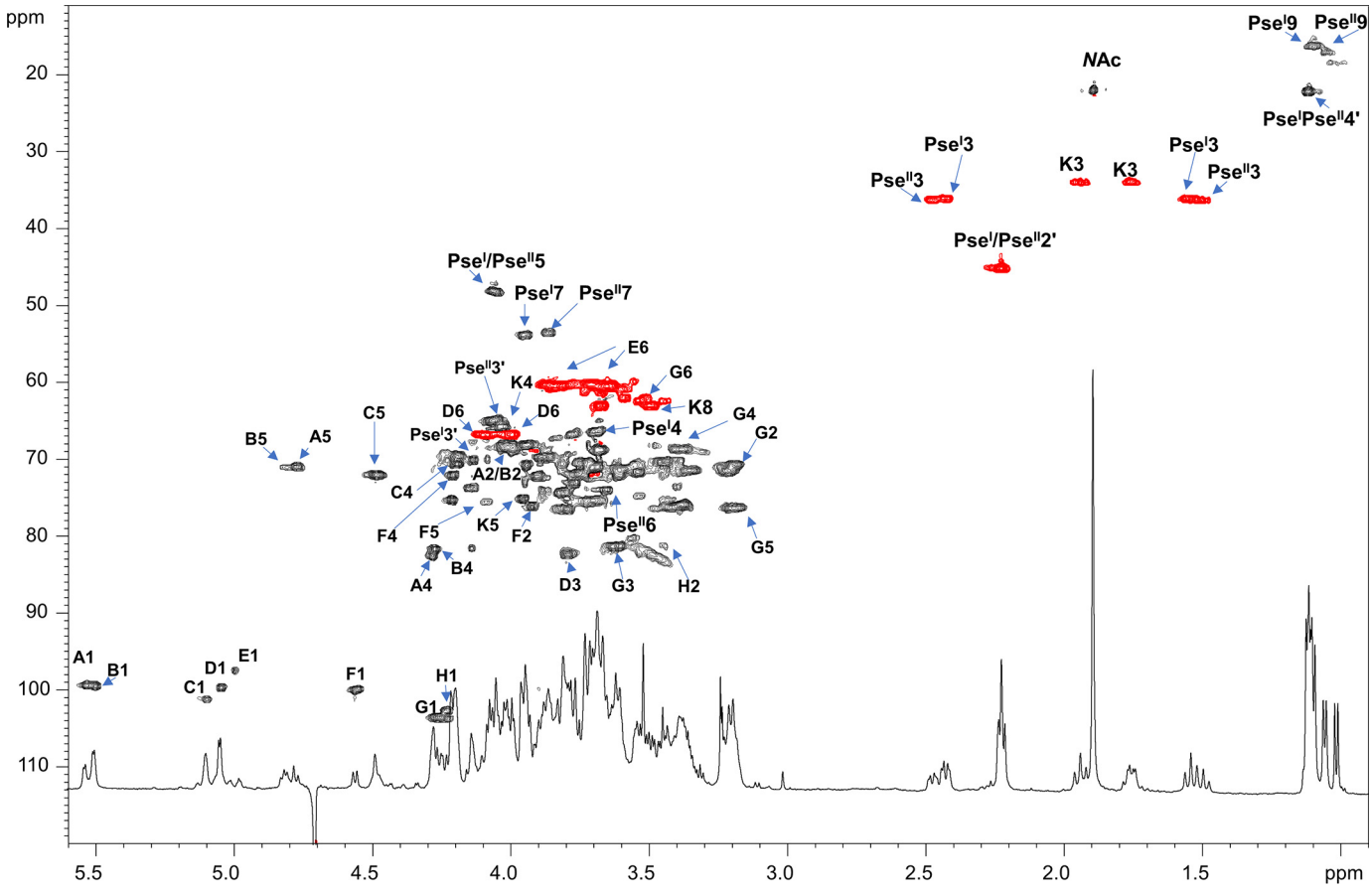

Figure 3. Zoom of the ^{1}H-^{13}C HSQC spectrum of OS1$_{rkpA}$ product obtained after mild acid hydrolysis of the LPS from *S. fredii* HH103 *rkpA*. Most of the heteronuclear correlations are indicated. Spin system labels are indicated as described in Table 2. The color of the cross-peaks indicates the phase: *black* indicates CH and CH_3 signals, whereas *red* indicates CH_2 signals.

MALDI-TOF MS of intact LPS from HH103 rkpA and rkpM mutants

An aliquot of pure LPS isolated from HH103 *rkpA* and HH103 *rkpM* has been investigated by MALDI-TOF MS. The MS spectra, recorded in negative polarity, are reported in Fig. 6. The linear MALDI-TOF MS spectrum of HH103 *rkpA* LPS (Fig. 6*A*) showed at higher molecular masses (between *m*/*z* 3500 and 4800) a series of $[M–H]^-$ ions relative to the native LPS mixture, composed of species differing by the composition of both the acyl and the sugar moieties. More importantly, ion fragments arising from the cleavage of the labile glycosidic bond between Kdo and the lipid A portion were also identified at lower mass ranges (*m*/*z* 1500–2100). This LPS fragmentation (*β*-elimination) yielding both oligosaccharide ions and lipid A ions furnished important details about the structure of HH103 *rkpA* LPS. In particular, the MALDI-TOF MS investigation gave us the chance to appreciate the heterogeneity of both the lipid A and the core OS portion of such LPS. Indeed, the main ion fragments in Fig. 6*A* at *m*/*z* 1770.2 corresponded to an OS composed of four hexuronic acids (HexA), three hexoses (Hex), one Kdo, and one Pse (**OS$_A$**), namely, an OS species matching with the one identified in the NMR analysis but lacking one Pse and one HexA unit. More interestingly, the ion fragment at *m*/*z* 2165.7 was attributed to an OS made up of five HexA, three Hex, two Kdo, and one Pse (**OS$_B$**), confirming the occurrence of a second unit of Kdo, as observed in the NMR investigation of the fully deacylated product. Finally, the main LPS species, as stated above, were consistent with a combination of the OS ion peaks and differently acylated lipid A species.

Similarly, the reflectron MALDI-TOF MS spectrum of intact LPS from the HH103 *rkpM* mutant revealed the occurrence of a main fragment ion at *m*/*z* 1409.5 relative to an OS built up of four HexA, three Hex, and one Kdo (**OS$_A$**); OS fragments composed by a further Kdo unit (*m*/*z* 1629.7, **OS$_B$**) and HexA (*m*/*z* 1805.5, **OS$_C$**) have also been identified. Therefore, by MALDI-TOF MS analysis it was possible to further confirm that HH103 *rkpM* expresses an LPS devoid of Pse, according to NMR data. As described for the *rkpA* mutant, in the higher mass region, LPS species composed of the above OS species and differently acylated lipid A forms have been detected.

Fatty acid compositional analysis and MALDI-TOF MS of lipid A from HH103 rkpM and rkpA LPS

Fatty acid compositional analysis revealed the occurrence, in both HH103 mutants, of 12:0(3-OH), 13:0(3-OH), 14:0(3-OH), 15:0(3-OH), 16:0(3-OH), 17:0(3-OH), 18:0(3-OH), 19:0(3-OH), 18:1(3-OH), 18:2(3-OH), 19:1(3-OH), 20:1(3-OH), and the very-long-chain fatty acids (VLCFA) 28:0(27-OH), 30:0(29-OH), 28:0(27-OHBu), and 30:0(29-OHBu), which is consistent with the lipid A fatty acid composition from the genus

Table 2

Proton and carbon chemical shifts of the OS1$_{rkpA}$ (A-H, K, Pse^{I} and Pse^{II}) and OS2$_{rkpA}$ (E_2, K_2, J, X, and Y) products derived from mild acid hydrolysis and complete deacylation, respectively, of LPS from *S. fredii* HH103 *rkpA*

Product	Chemical shift	Value at position[a]:								
		1/1′	2/2′	3/3′	4/4′	5	6	7	8	9
A	^{1}H	5.53	4.03	3.69	4.28	4.77				
4-α-D-GalA	^{13}C	99.4	68.3	71.0	82.5	71.1	175.3			
B	^{1}H	5.50	3.99	3.68	4.27	4.81				
4-α-D-GalA	^{13}C	99.5	68.4	71.0	81.6	71.0	175.1			
C	^{1}H	5.09	3.68	3.88	4.19	4.49				
t-α-D-GlcA	^{13}C	101.2	68.7	69.5	70.5	71.9	175.5			
D	^{1}H	5.04	3.53	3.79	4.19	3.91	4.09/3.99			
3,6-α-D-Gal	^{13}C	99.7	71.6	82.3	69.5	70.4	66.7			
E	^{1}H	5.00	3.45	3.75	3.38	3.95	3.84/3.64			
t-α-D-Glc	^{13}C	97.4	70.3	70.5	70.3	72.9	60.4			
F	^{1}H	4.55	3.92	3.88	4.20	4.07				
2-β-D-GalA	^{13}C	99.9	76.2	74.0	72.1	75.4	175.4			
G	^{1}H	4.26	3.18	3.62	3.38	3.19	3.52			
3-β-D-Glc	^{13}C	103.5	70.7	81.1	68.5	76.2	62.2			
H	^{1}H	4.23	3.44	3.40	3.31	3.42				
2-β-D-GlcA	^{13}C	102.6	81.3	76.1	68.9	76.0	174.2			
K	^{1}H			1.94/1.75	4.03	3.95	3.69	3.87	3.67/3.49	
4,5-α-D-Kdo	^{13}C	ND	96.2	33.9	65.5	75.0	70.9	69.7	63.0	
Pse^{I}	^{1}H			2.42/1.55	3.68	4.05	3.77	3.94	4.01	1.09
3′-β-L,L-Pse	^{13}C	172.8	103.2	36.0	66.3	48.0	73.0	53.7	68.3	16.2
HBu	^{1}H		2.24	4.13	1.13					
	^{13}C	173.4	45.0	69.8	22.0					
Pse^{II}	^{1}H			2.47/1.50	3.77	4.05	3.65	3.86	3.99	1.05
t-β-L,L-Pse	^{13}C	172.1	102.3	36.1	66.6	48.0	73.9	53.5	68.8	16.9
HBu	^{1}H		2.22	4.06	1.11					
	^{13}C	173.3	44.9	64.8	21.9					
*N*Ac						1.90				
						21.8				
X	^{1}H	5.55	3.30	3.80	3.47	4.06	4.16/3.68			
6-α-D-GlcN	^{13}C	90.4	54.1	69.5	70.1	72.4	69.2			
Y	^{1}H	4.78	2.95	3.71	3.40	3.67	3.44			
6-β-D-GlcN	^{13}C	99.3	55.5	71.9	69.6	75.0	61.0			
E_2	^{1}H	5.08	3.68	3.68	3.26	4.06	3.43			
2-α-D-Glc	^{13}C	97.3	75.4	71.9	69.8	72.0	61.0			
K_2	^{1}H			1.74/1.99	4.05	4.20	3.62	3.92	3.82/3.55	
4,5-α-D-Kdo	^{13}C	ND	ND	34.3	70.4	72.2	72.2	70.3	62.8	
J	^{1}H			1.86/2.11	3.83	3.91	3.93	3.87	3.82/3.49	
t-α-D-Kdo	^{13}C	ND	ND	33.9	69.4	70.1	71.4	69.6	63.0	

[a] 1′, 2′, 3′, and 4′ indicate the proton and the carbon positions of the HBu group. The proton chemical shift of the NH of the NAc group for both **Pse^{I}** and **Pse^{II}** was at 7.51 ppm, whereas that at position 7 of both **Pse^{I}** and **Pse^{II}** was at 7.18 ppm.

Sinorhizobium (23). To unveil the structure of the glycolipid portion of the LPS from both mutants, an aliquot of the mild acid hydrolysis-precipitated product, containing lipid A, has been analyzed by negative-ion MALDI-TOF MS (the spectrum is reported in Fig. S3, *A* and *B*). The MALDI mass spectra of the isolated lipid A fractions were identical for both mutants and further confirmed, and expanded on, the high heterogeneity of such LPS moieties and the occurrence of hydroxybutyrate as an acyloxyacyl substituent carried on some of the VLCFAs. The main ion peaks and the proposed interpretation of the substituting fatty acids on the lipid A backbone are reported in Table S2. As an example, in the higher mass regions, the ion peak at *m*/*z* 2066.0 was attributed to a *bis*-phosphorylated penta-acylated lipid A species carrying two 14:0(3-OH), one 18:0(3-OH), and one 19:0(3-OH) as primary fatty acids and one 30:0(29-OHBu) as the secondary acyl moiety; further on, the ion peak at *m*/*z* 1952.0 corresponded to a penta-acylated lipid A species decorated by two phosphates and carrying two 14:0(3-OH), one 18:0(3-OH), one 19:0(3-OH), and one 28:0(27-OH), whose relative species missing one 14:0(3-OH) was assigned to a peak at *m*/*z* 1725.9. At *m*/*z* 2050.0, a further penta-acylated lipid A form decorated by two phosphates, two 14:0(3-OH), one 18:0 (3-OH), one 18:1(3-OH), and one 30:0(29-OHBu) was also detected (Fig. S3*C*); the related species carrying only one phosphate group and lacking one 14:0(3-OH) moiety was identified at *m*/*z* 1743.9. The more intense ion peak at *m*/*z* 1870.0 was assigned to *bis*-phosphorylated lipid A forms composed of two 14:0(3-OH), one 13:0(3-OH), one 12:0(3-OH), and one 28:0(27-OHBu), whose relative species lacking one 14:0(3-OH) was identified at *m*/*z* 1643.9.

The mAb NB6-228.22 recognizes S. fredii HH103 Rif^{R} LPS but fails in the recognition of KPS

Structural investigation demonstrated that a β-configured Pse5NAc7(3OHBu) is present in the LPS of *rkpA* but absent from *rkpM*. Because NB6-228.22 binds to the LPS produced by *rkpA* but fails in the recognition of *rkpM* LPS, we investigated whether this mAb was also able to recognize the KPS produced by HH103 Rif^{R}, which is a homopolymer of α-Pse5NAc7 (3OHBu) (12).

For this purpose, intact cells of *S. fredii* HH103 Rif^{R} and its derivatives mutated in the *rkpA*, *rkpM*, *rkpK*, *lpsL*, *lpsB*, and *lpsE* genes were transferred to a nylon membrane and were deposited on a positively charged nylon transfer membrane and immunostained with NB6-228.22. In this experiment, purified LPS and KPS samples from HH103 were also analyzed. As shown in Fig. 7*A*, only cells from the two strains not affected in

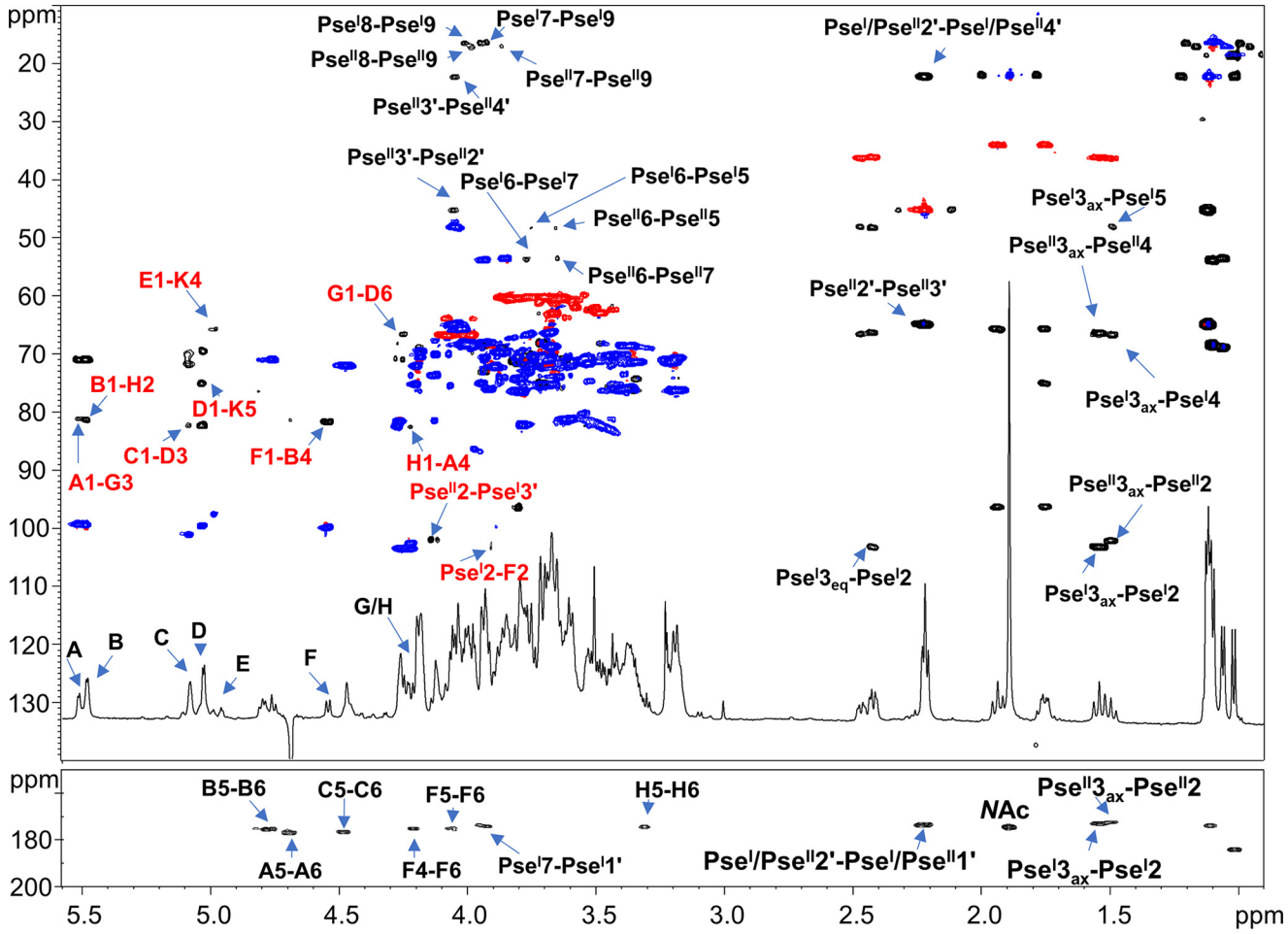

Figure 4. Superimposition of ^{1}H-^{13}C HSQC (*blue*/*red*) with ^{1}H-^{13}C HMBC (*black*) of OS1$_{rkpA}$ product. Densities are labeled with the same letters listed in Table 2. The most relevant interresidue long-range correlations involving sugar moieties are indicated in *red*, whereas in *black* are reported some important intraresidue long-range correlations.

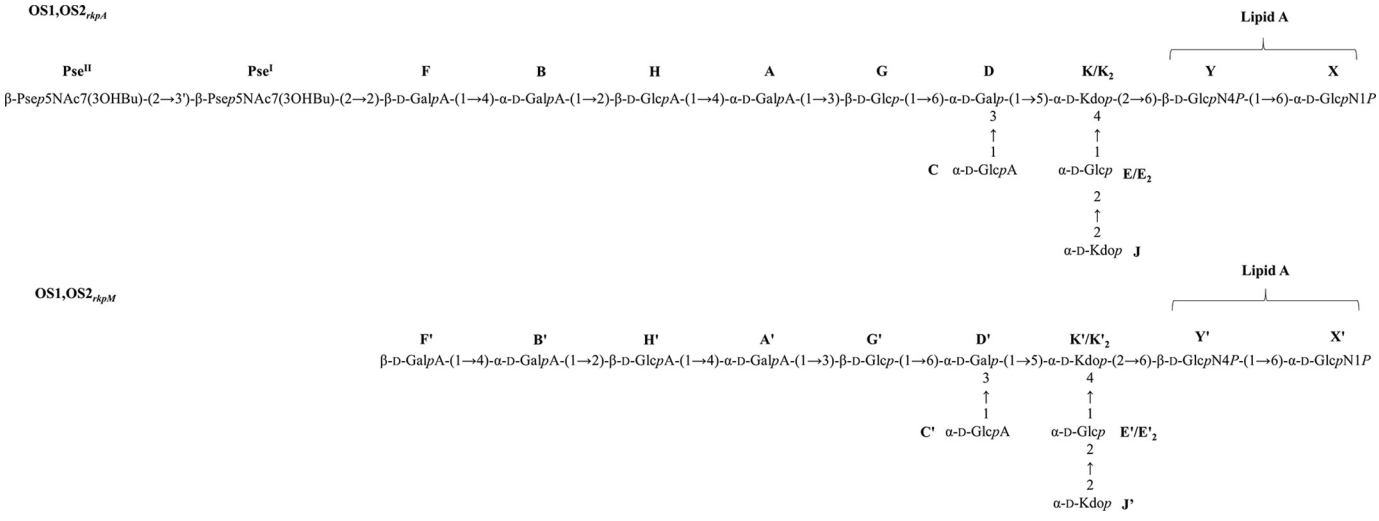

Figure 5. Structural assessments of the OS1$_{rkpA}$, OS2$_{rkpA}$, OS1$_{rkpM}$, and OS2$_{rkpM}$ products. The complete structure of the core OS from *S. fredii* HH103 *rkpA* and *rkpM* was achieved by combination of data attained from the NMR investigation of the LPS after mild acid hydrolysis (yielding **OS1**$_{rkpA}$ and **OS1**$_{rkpM}$) and full deacylation (yielding **OS2**$_{rkpA}$ and **OS2**$_{rkpM}$) procedures. The mild acid hydrolysis selectively cleaved the linkage between the Kdo and the nonreducing glucosamine of the lipid A portion, enabling the isolation of the core OS moieties (sugar units labeled **A**, **A'**-**H**, **H'**, **K**, **K'**, **Pse^{I}**, and **Pse^{II}**) from the lipid A domain. The complete deacylation procedure allowed the isolation of the core OS plus the glucosamine disaccharide backbone (labeled **X**, **X'**, **Y**, and **Y'**) of the lipid A. The occurrence of an additional Kdo unit (**J**, **J'**) was deduced by analysis of the fully deacylated products which, consequently, allowed the identification of the spin system **E$_2$**, **E$_2$'** (*i.e.* the α-D-Glc*p* substituted at position 2 by the Kdo unit **J**, **J'**). The core OS structures are labeled using letters in Table 2 and Table S2. *p* indicates the pyranose form of sugar residues, whereas *P* indicates the phosphate group.

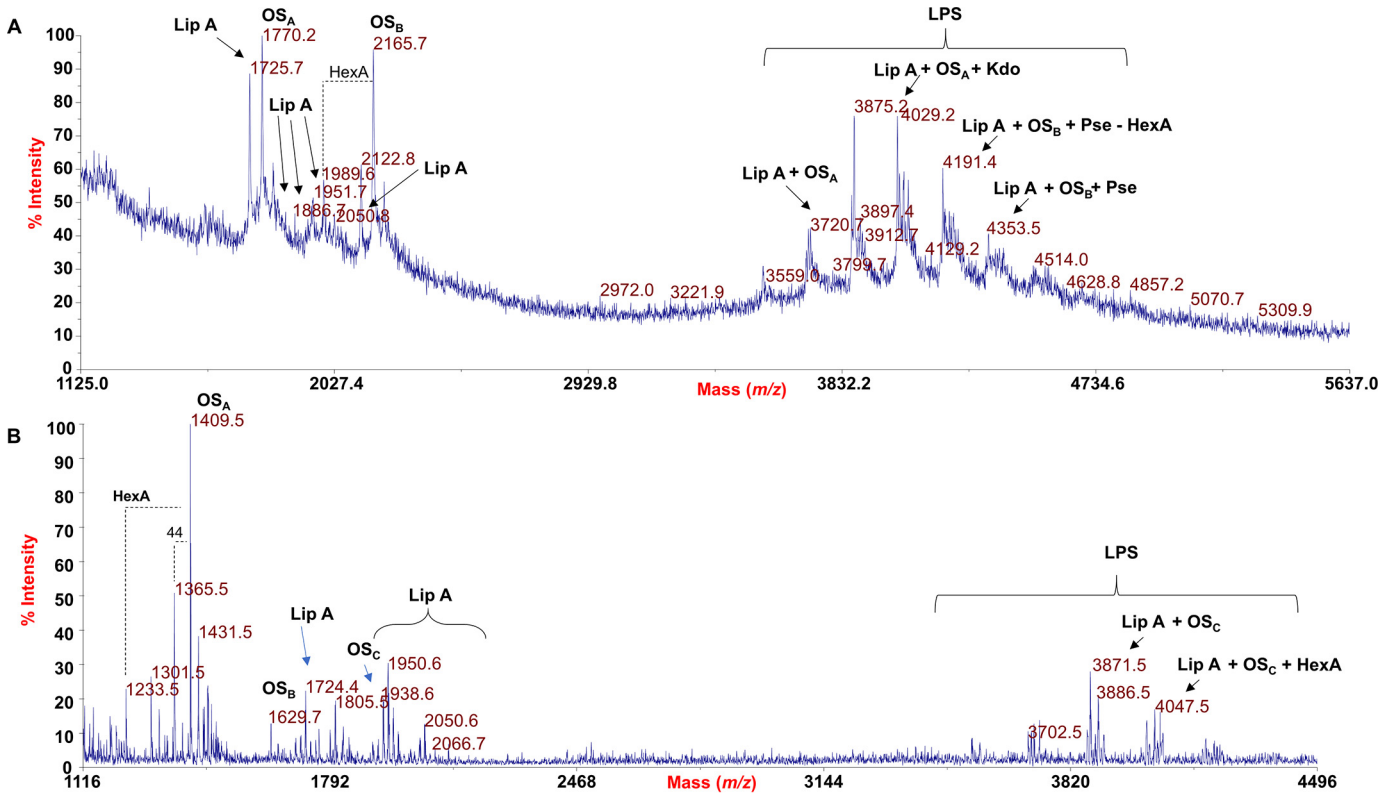

Figure 6. ***A*, negative-ion MALDI mass spectrum of intact LPS from *S. fredii* HH103 *rkpA* recorded in linear mode.** Both LPS molecular ions and their ion fragments, attributable to the core OS (**OS_A, OS_B**) and lipid A (**LipA**) species, are visible and indicated in the spectrum. *B*, negative-ion MALDI mass spectrum of LPS of *S. fredii* HH103 mutant *rkpM* recorded in reflectron mode. The lipid A (**LipA**) and core OS (**OS_A, OS_B, OS_C**) species are also indicated in the spectrum. Proposed structural assessment of some LPS-related ions has been reported.

their LPS (HH103 and its *rkpA* derivative) as well as the purified LPS sample showed positive recognition by NB6-228.22. These results clearly indicate that NB6-228.22 does not react with HH103 KPS.

The epitope recognized by the mAb NB6-228.22 is not common in S. fredii strains

Both the LPS and KPS structures may vary at the strain level (1, 19). For this reason, we decided to investigate the reactivity of other *S. fredii* strains against NB6-228.22. Intact cells of 25 *S. fredii* strains (including HH103) that have been isolated in previous works from soybean plants growing in soils of different Chinese provinces were included in this study (Table S3, Fig. 7*B*). Only two of these strains (HH103 and HH102), which were isolated from nodules of soybean plants inoculated with soil from Hubei province (43), were recognized by the antibody. The remaining tested strains, isolated and reported in the period 1982–2003 (44), from soils of Chinese East-Central provinces (Shanghai, Hubei, Henan, and Shandong), as well as from the Xingjian Autonomous Region (Western China), were not recognized by NB6-228.22. *S. fredii* NGR234 and *S. meliloti* AK631 were included in this study, because their KPS contain two different derivatives of the pseudaminic acid (45). Intact cells of NGR234 and AK631 were not recognized by NB6-228.22 (Fig. 7*B*). Immunostaining of PAGE-separated LPS samples from several *S. fredii* strains confirmed that NB6-228.22 recognized the different LPS bands from HH102 but failed to recognize LPS from strains HGW35, B33, USDA196, USDA197, USDA205, and USDA208 (Fig. 7*C*).

Because the *rkp-3* region is involved in the production of Pse5NAc7(3OHBu) (17), all the *S. fredii* strains tested with NB6-228.22 were also investigated by PCR for the presence of the *rkpL*, *rkpM*, *rkpP*, and *rkpQ* genes using genomic DNA (gDNA) as the template (Tables S3 and S4). Strain NGR234 was not included in these experiments because its *rkp-3* region has been sequenced (46). Only the gDNA of HH103 and HH102 led to the amplification of the expected fragments for all the genes investigated (Table S3), whereas when gDNA of strain S50 was used, the internal fragments of *rkpM* and *rkpP*, but not those of *rkpL* and *rkpQ*, could be amplified. All amplified fragments showed an identity of 98–100% with the corresponding *rkp* gene of *S. fredii* HH103 Rif^R (Table S4).

Because *S. fredii* S50 appeared to have only part of the *rkpLMNOPQ* operon, we investigated the presence of these genes in sinorhizobial strains for which sequences homologous (>85.0 identity at amino acid level) to RkpM were found *in silico*. The complete operon was present in *S. fredii* CCBAU05631, *Sinorhizobium* sp. strain BJ1, *S. meliloti* Rm41, *S. medicae* Str9, and *S. americanum* CCGM7 (Table S5). In two other strains, *S. fredii* NGR234 and *S. saheli* LMG7837, the *rkpP* genes were missing. *S. fredii* strain CCBAU45436 lacks *rkpO*, and the rest of the predicted proteins showed identities lower than 55%. Figure 8 shows the organization of the *rkp-3* region in *S. fredii* strains as well as in *S. meliloti* Rm41.

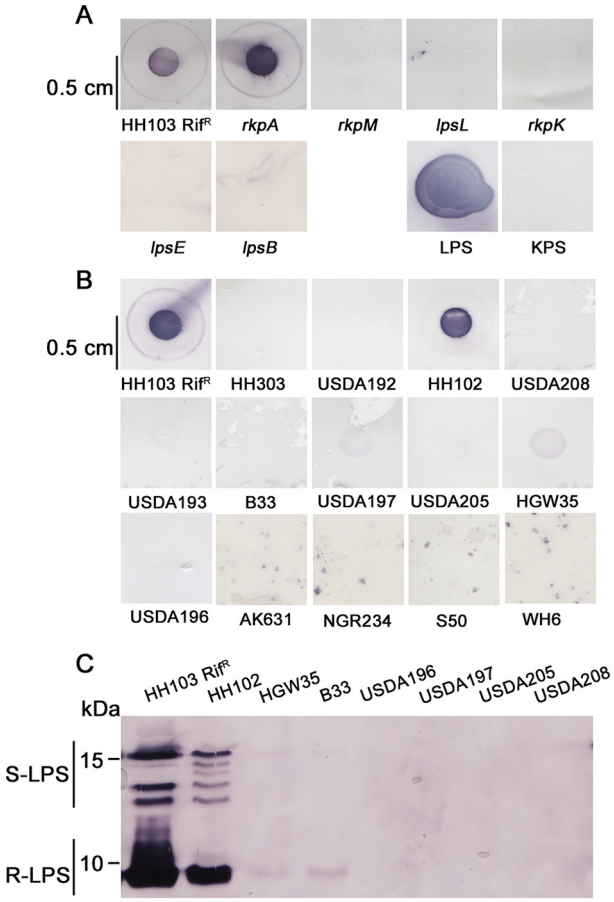

Figure 7. *A*, immunostaining of intact cells of *S. fredii* HH103 Rif^R and HH103 mutants in the *rkpA*, *rkpM*, *rkpK*, *lpsL*, *lpsB*, and *lpsE* genes using the mAb NB6-228.22. *LPS*, sample containing HH103 Rif^R crude extract preparations used for PAGE electrophoresis (they contain KPS and LPS). *KPS*, sample containing HH103 *lpsB* KPS. *B*, immunostaining of intact cells of *S. fredii* strains isolated from diverse geographical areas and *S. meliloti* AK631. *C*, immunostaining of LPS electrophoretic patterns of diverse *S. fredii* strains.

The symbiotic impairment of the S. fredii HH103 rkpM mutant is higher with Cajanus cajan than with Macroptilium atropurpureum

The symbiotic relevance of LPS and KPS in rhizobium-legume interactions has been extensively documented (1–5). In this work, we have analyzed the symbiotic phenotype of HH103 *rkpM* and its complemented version, HH103 *rkpM* C, with two HH103 host legumes, *M. atropupureum* and *C. cajan*, which form determinate and indeterminate nodules, respectively (17, 38).

In the case of *M. atropurpureum* (Table 3 and Fig. 9), HH103 *rkpA*, affected in KPS but not in LPS production, was also included in these studies. The number and fresh weight of nodules of *M. atropurpureum* plants inoculated with HH103 *rkpA* or HH103 *rkpM* were similar and significantly lower than those formed on plants inoculated with HH103 Rif^R, although nodules induced by HH103 *rkpM* were white. Plants inoculated with these mutants were stunted with yellow leaves, and their plant-top dry weight was not significantly different from that of the uninoculated control. In contrast, plants inoculated with HH103 Rif^R or HH103 *rkpM* C produced green leaves and plants did not show symptoms of nitrogen starvation. Nitrogenase activity (nmol ethylene/3 plants × hour, determined by acetylene reduction assays) was similar in plants growing in the three jars inoculated with HH103 Rif^R (136 ± 43) or HH103 *rkpM* C (154 ± 63) and lower in the three jars inoculated with HH103 *rkpA* (36 ± 14). When HH103 *rkpM* was used as the inoculant, a very low nitrogenase activity could be detected and only in two out of the three jars analyzed (4.7 and 15.1). Microscopy analyses showed dispersed patches of nodule cells invaded by HH103 *rkpM* (Fig. 10*A2*), which contained less bacteroids than those infected by *S. fredii* HH103 Rif^R or HH103 *rkpM* C (Fig. 10*A1* and *A3*). Nodules induced by HH103 *rkpA* (Fig. 10*A4*) showed an infection level that could be considered an intermediate stage between those induced by HH103 Rif^R and HH103 *rkpM*.

The symbiotic impairment of another *rkpM* mutant (called SVQ582) with *C. cajan* was previously reported (17), although microscopy of the pseudonodules produced was not carried out. Because infected cells were found in *M. atropurpureum* nodules, we investigated whether *C. cajan* pseudonodules contained cells invaded by the HH103 *rkpM* mutant investigated in the present work. Plant-top dry weight of *C. cajan* plants inoculated with HH103 *rkpM* was not significantly different from that shown by uninoculated controls (78 and 101 mg/plant, respectively). Plants inoculated with HH103 *rkpM* only formed pseudonodules and macroscopic swellings (Table 3, Fig. 9). Microscopy images showed that pseudonodules induced by this mutant were devoid of bacteroids (Fig. 10*B2*). *C. cajan* plants inoculated with *S. fredii* HH103 Rif^R or HH103 *rkpM* C formed nitrogen-fixing nodules, and plants were green and did not show symptoms of nitrogen starvation (Fig. 9).

Discussion

In this work, we report the characterization of the full structure of the LPS from *S. fredii* HH103 *rkpA*. We selected this mutant because its LPS shows the same electrophoretic profile and reactivity with the mAb NB6-228.22 as the WT strain LPS does. Thus, the LPS structure of HH103 *rkpA* is assumed to be equal to that of the WT strain. In addition, HH103 *rkpA* is devoid of KPS, a polysaccharide that can interfere with LPS purification procedures. Our work reveals a novel core OS with a high content in hexuronic acids and showing the presence of β-Pse5NAc7(3OHBu) located at the outermost part of the LPS. This residue was found to be linked to another one of the same nature, which might constitute an extremely short O-chain moiety (Fig. 5). In previous works, we obtained different HH103 mutants affected in LPS structure, as reflected in their altered electrophoretic profiles (Table 1) (17, 31, 37). In this work, we have also carried out the structural analysis of the LPS produced by HH103 *rkpM*, because its LPS electrophoretic profile was less altered than that of HH103 LPS, among the different HH103 mutants available. Our work highlights that the core OS of HH103 *rkpM* lacks Pse5NAc7(3OHBu) (Fig. 5). This result is in full accordance with the fact that the *rkpLMNOPQ* operon is involved in the biosynthesis of Pse derivatives in *S. meliloti* 41 (47) and *S. fredii* HH103 (17). Finally, the lipid A moieties of both *rkpA* and *rkpM* were found

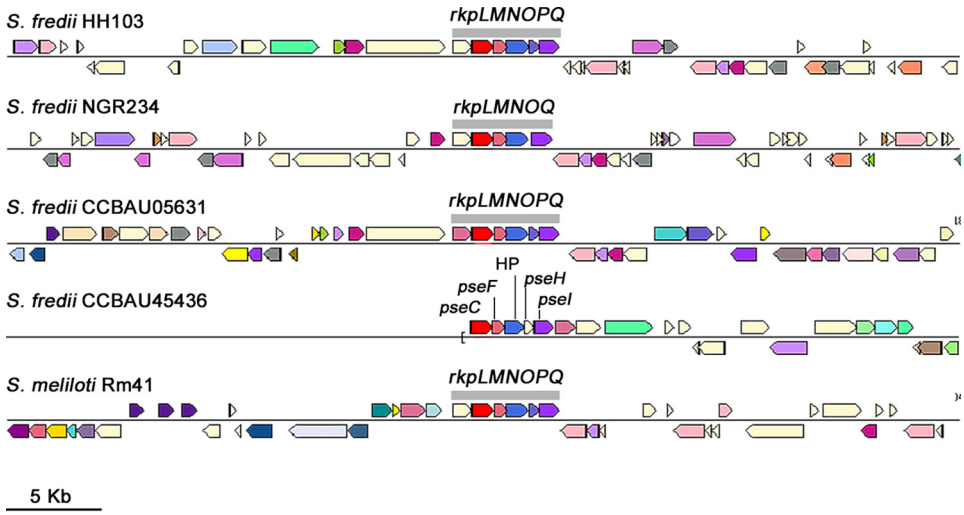

Figure 8. The *rkp*-3 region organization in the different *S. fredii* strains analyzed and *S. meliloti* Rm41 as a reference. Genes in *red* correspond to the *rkpM* gene or, in the case of CCBAU45436, to an orthologue with similar function. The *rkp-3* genes shown have different colors depending on their function.

Table 3

***Macroptilium atropurpureum* and *Cajanus cajan* responses to inoculation with *S. fredii* HH103 Rif^R, its *rkpM* mutant, and its complemented derivative[a] (HH103 *rkpM* C)**

Legume and inoculant	No. of nodules	Fresh wt of nodules (mg)	Plant-top dry wt (mg)
Macroptilium atropurpureum			
HH103 Rif^R	39.00 ± 4.77 A	50.53 ± 4.8 A	127.61 ± 10.03 A
HH103 *rkpM*	4.33 ± 0.47 B	13.84 ± 2.39 B	41.43 ± 4.56 B
HH103 *rkpM* C	30.00 ± 2.22 A	48.78 ± 4.68 A	110.15 ± 11.02 A
HH103 *rkpA*	8.45 ± 0.81 B	17.53 ± 3.37 B	63.45 ± 6.23 B
Uninoculated	None		48.83 ± 2.78 B
Cajanus cajan			
HH103 Rif^R	30.58 ± 1.15 A	273.84 ± 33.84 A	621.22 ± 59.35 A
HH103 *rkpM*	Pseudonodules		78.68 ± 5.04 B
HH103 *rkpM* C	31.58 ± 3.17 A	353.95 ± 54.42 A	722.41 ± 89.13 A
Uninoculated	None		101.88 ± 10.72 B

[a]Numbers are mean (±S.E.) values per plant. *M. atropurpureum* roots inoculated with HH103 *rkpM* also developed pseudonodules. Twelve plants were analyzed for each legume/inoculant combination. For each legume, data in the same column with the same letter were not significantly different (one-way analysis of variance, α = 5%). For number of nodules, only those treatments showing nodules were compared.

to be identical and displayed a high degree of heterogeneity in the acyl chains, which were characterized by the nonstoichiometric substitution by hydroxybutyrate on the VLCFA and by the occurrence of unsaturated chains, as previously reported for other *Sinorhizobium* strains (23). The lack of function of RkpM also affects the alterations that the *S. fredii* HH103 LPS undergoes during bacteroid development in nodules of *Glycyrrhiza uralensis*.

The HH103 *lpsB*, *lpsE*, *lpsL*, and *rkpK* mutants are also presumably affected in the core structure of their LPS. LpsB and LpsE are predicted glycosyl transferases (31), whereas LpsL and RkpK are responsible for the synthesis of GalA and GlcA, respectively, (37), and, as demonstrated in the present work, the HH103 LPS core contains hexoses and these two uronic acids. We planned to analyze the LPS structure of these four HH103 LPS mutants in the future.

The mAb NB6-228.22 recognizes all of the LPS silver-stained bands of WT HH103 and its *rkpA* mutant derivative (unable to produce KPS) as well as entire cells of these two strains and a purified HH103 LPS sample. However, it failed to perceive the LPS of HH103 *rkpM*, which strongly suggested that the Pse5NAc7(3OHBu) residue present in the LPS core OS of HH103 and HH103 *rkpA* should be the epitope (or part of it) recognized by this antibody. Interestingly, antibody NB6-228.22 failed to perceive a purified sample of the *S. fredii* HH103 KPS, even though Pse5NAc7(3OHBu) is the only component of this polysaccharide, and failed in the recognition of intact cells and LPS profiles of HH103 *lpsL*, *lpsB*, *lpsE*, and *rkpK* mutants (altered LPS, WT KPS). Thus, it was possible to conclude that the mAb NB6-228.22 recognizes the HH103 LPS but not its KPS. There are various possibilities that could explain why the same monosaccharide, Pse5NAc7(3OHBu), is recognized in the LPS but not in the KPS. One very likely explanation is that Pse5NAc7(3OHBu) residues are α-linked in the KPS (12) but β-linked in the LPS. Alternatively, the epitope perceived by the antibody might not be restricted to only Pse5NAc7(3OHBu), which is the case of the HH103 Rif^R KPS but not of the LPS in which Pse5NAc7(3OHBu) is linked to a D-GalA residue (Fig. 5). In any case, the epitope recognized by the antibody NB6-228.22 is infrequent in *S. fredii* strains, as demonstrated by the fact that only 2 of 25 strains analyzed (including HH103) reacted with this antibody. This fact is not unexpected, because the LPS core and O-antigen regions are known to vary at the strain level (1, 19).

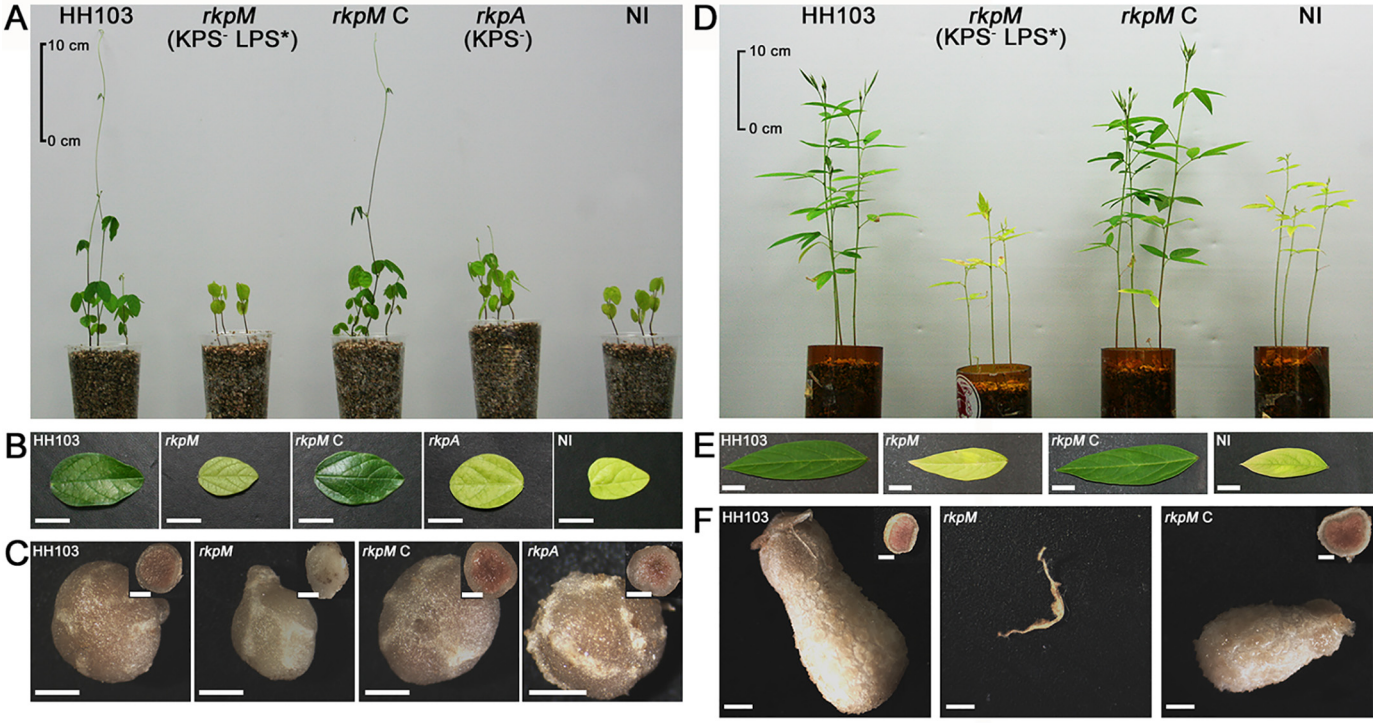

Figure 9. Symbiotic performance of HH103 *rkpM* and its complemented version (HH103 *rkpM* C) with *Macroptilium atropurpureum* (*A–C*) and *Cajanus cajan* (*D–F*). The HH103 *rkpA* mutant was also included in the studies with *M. atropurpureum*. The WT strain is denoted as HH103. *NI* stands for noninoculated plants. The phenotype regarding surface polysaccharide production of mutants *rkpM* and *rkpA* is shown is *panels A* and *D*. *LPS** indicates production of an altered LPS. *A* and *D*, aerial part of the plants at the end of the assay. *B* and *E*, plant leaves. *C* and *F*, complete and transversal sections of nodules (or macroscopic root outgrowths) induced by inoculation with the different strains. The *bars* in *B* and *E* correspond to 1 cm and in *C* and *F* to 1 mm.

PCR experiments and *in silico* analyses carried out in this work showed that the *rkpLMNOPQ* operon involved in Pse5NAc7(3OHBu) biosynthesis can be found in diverse *Sinorhizobium* species, but its presence might not be frequent at the strain level. In addition, some of the *Sinorhizobium* strains containing the region lack some of these genes. *S. fredii* S50 amplified the *rkpM* and *rkpP* genes but failed in the amplification of *rkpQ* and *rkpL*. The amplified internal sequences of S50 *rkpM* and *rkpP* are nearly identical to those of HH103 (98–100% identity), which suggests that the failure to amplify *rkpQ* and *rkpL* is because of the absence of these genes in S50 rather than the unsuitable nucleotide sequences of the primers used. *S. fredii* NGR234 and *S. saheli* LMG7837 are devoid of orthologues of *rkpP*, and *S. fredii* CCBAU45436 lacks *rkpO*. The absence of *rkpP* does not prevent the biosynthesis of the Pse derivative present in the NGR234 KPS (46).

In previous studies, we showed that two plants forming determinate nodules, soybean and cowpea (*Vigna unguiculata*), when inoculated with HH103 *rkpM* only formed pseudonodules that did not fix nitrogen and were devoid of intracellular bacteria, whereas this mutant was able to induce the formation of Fix^+ nodules with *Lotus burttii* (determinate nodules) and *Glycyrrhiza uralensis* (indeterminate nodules) (17, 48). In this work, we have included another determinate-nodule forming legume, *Macroptilium atropurpureum*, and showed that nodulation of plants inoculated with HH103 *rkpM* was severely reduced and nitrogen fixation almost abolished compared with those inoculated with HH103 (Table 3).

In contrast to HH103 *rkpM*, *S. fredii* HH103 *lpsB* and *lpsE* mutants (presenting KPS but with an altered LPS) as well as *S. fredii* HH103 mutants in genes of the *rkp-1* region (unable to produce KPS but with a normal LPS) are still able to induce the formation of Fix^+ nodules in both soybean and cowpea plants, albeit nodulation is reduced and plants show symptoms of nitrogen starvation (14–17). Considering all these results, we can conclude that in *S. fredii* HH103 the combination of the absence of KPS production and an alteration of the LPS, consisting of the absence of Pse5NAc7(3OHBu), causes the most severe symbiotic impairment with these two legumes. An *S. fredii* HH103 Rif^R double (*rkpH* and *exoA*) mutant unable to produce KPS and EPS (LPS electrophoretic profile apparently unaffected) was still able to induce the formation of some nitrogen-fixing nodules with *G. max* cvs. Williams and Peking (14). Thus, the loss of EPS production in an *S. fredii* HH103 unable to produce KPS is not so harmful for the bacterial symbiotic capacity with soybeans than the simultaneous absence of KPS production and Pse5NAc7(3OHBu) residues in the LPS structure.

Thus, two types of plant responses to inoculation with HH103 *rkpM* can be observed in both determinate and indeterminate nodules forming legumes: *G. max*, *V. unguiculata*, and C. *cajan* formed uninfected pseudonodules, whereas *L. burttii*, *M. atropurpureum*, and *G. uralensis* were still able to form a variable number of nitrogen-fixing nodules. All these results indicate that the symbiotic impairment of mutations affecting *S. fredii* HH103 surface polysaccharides vary among the

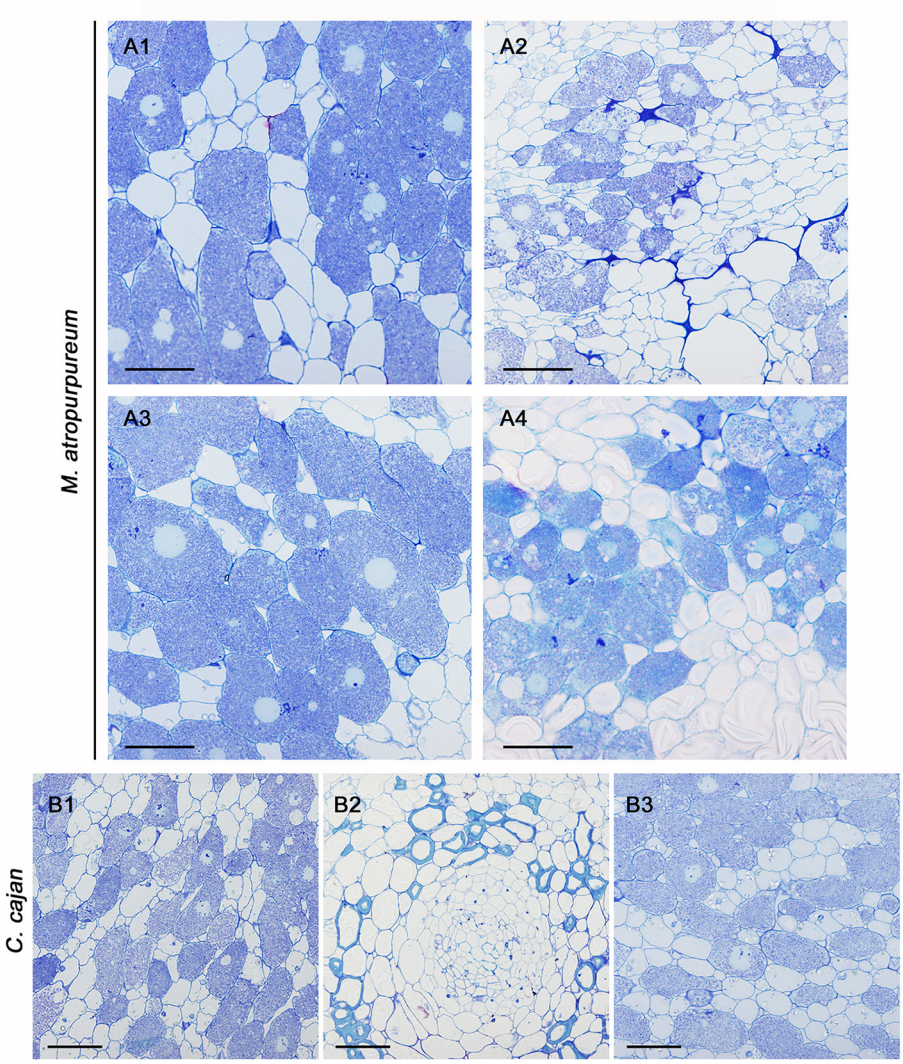

Figure 10. Structure of *Macroptilium atropurpureum* and *Cajanus cajan* nodules elicited by inoculation with *S. fredii* HH103, its *rkpM* and *rkpA* mutants, and the *rkpM* complemented strain (HH103 *rkpM* C). *M. atropurpureum* nodules induced by HH103 Rif^R (*A1*), HH103 *rkpM* (*A2*), HH103 *rkpM* complemented (HH103 *rkpM* C, *A3*), and HH103 *rkpA* (*A4*). *C. cajan* nodules or pseudonodules were elicited by HH103 Rif^R (*B1*), HH103 *rkpM* (*B2*), and HH103 *rkpM* C (*B3*). Nodules were analyzed seven (*M. atropurpureum*) or eight (*C. cajan*) weeks after inoculation. The b*ar size* represents 50 μm.

different legumes tested, regardless of whether they form indeterminate or determinate nodules, and that the simultaneous alteration of two polysaccharides can produce unpredictable impacts on the bacterial symbiotic capacity.

RSP, such as LPS and KPS, also can be important for stress tolerance both under free-living conditions and during the infection process and bacteroid persistence (29, 31, 49). Here, we have studied the effect of the *rkpA* and *rkpM* mutations on the final growth (expressed as the optical density at 600 nm [OD_{600}] scored 24, 48, or 120 h after inoculation) of *S. fredii* HH103 in liquid minimal medium supplemented with high concentrations of either sodium chloride (100 or 150 mM) or the detergent SDS (0.35 or 0.52 mM) (Fig. S4). No differences among the different strains were found in the presence of 100 or 150 mM NaCl or 0.35 mM SDS. However, 5 days after inoculation, the growth of *S. fredii* HH103 Rif^R and HH103 *rkpM* C in liquid MM supplemented with 0.52 mM SDS was higher (OD_{600}, >0.8) than that observed for HH103 *rkpM* (OD_{600} of about 0.3) or HH103 *rkpA* (OD_{600} of about 0.5) (Fig. S4). These results suggest that both KPS and LPS provide protection against SDS. Whether these phenotypes are related to the symbiotic impairment exhibited by HH103 *rkpM* requires further investigation.

In conclusion, with this work a novel LPS structure has been identified revealing the occurrence of an unprecedented component for rhizobial LPS, a β-configured Pse5NAc7(3OHBu), whose presence might be important for the establishment of an effective symbiosis of *S. fredii* HH103 with some of its host plants. This crucial point will be the object of future structure-to-function studies focused on the determination of the molecular motifs of *S. fredii* HH103 LPS that may be crucial for bacterium–plant cell interactions.

Experimental procedures

Extraction, purification, and SDS-PAGE analysis of rkpA and rkpM LPS

Dried bacterial cells of HH103 *rkpA* and *rkpM* were washed several times with distilled water, ethanol, acetone, and ethylic

ether to remove growth culture contaminants. After lyophilization, the bacterial pellets were extracted by the phenol/water method (40). After extensive dialyses against distilled water, the extracted phases were suspended in 40 ml of digestion buffer (100 mM Tris, 50 mM NaCl, 10 mM $MgCl_2$, pH 7.5) to which RNase (4 mg, R5503-Merck), DNase (4 mg, DN25-Merck), and proteases (4 mg) were added to remove nucleic acids and protein contaminants. Both the water and phenol fractions were checked by SDS-PAGE after silver staining; the LPS material, in both HH103 *rkpA* and *rkpM*, was found exclusively in the water phases. To further purify the samples, the LPSs were ultracentrifuged (4 °C, 208,000 × *g*, 16 h) and then subjected to size-exclusion chromatography on a Sephacryl S-300 (GE Healthcare, 1.5 by 90 cm, eluent of 50 mM NH_4HCO_3).

LPS extraction for PAGE and immune-staining analyses, as well as the separation on SDS-PAGE gels, silver staining, and immunostaining procedures with the mAb NB6-228.22 (class IgG 2b), were performed as described previously (38). Production of the mAb NB6-228.22 (class IgG 2b) was described by Buendía-Clavería and collaborators (38). Briefly, soybean nodule-derived bacteroids of HH103 were used to immunize male rats (line LOU/IAP), and spleen cells derived from these rats were fused to the myeloma line IR983F. NB6-228.22 recognizes all the LPS bands from HH103 free-living cells or HH103 bacteroids isolated from soybean nodules. NB6-228.22 was purified from the hybridoma culture supernatant.

Binding assays of intact *S. fredii* cells to NB6-228.22 were carried out as follows. A loop of *S. fredii* cells grown on solid TY for 4 days was suspended in 200 μl of sterile water. 10-μl drops of bacterial suspensions then were deposited on positively charged Nylon transfer membranes (Amersham Biosciences, UK). Intact bacterial samples absorbed to the filters were immunostained with NB6-288.22, using as the secondary antibody a goat anti-rat IgG conjugated to alkaline phosphatase (Sigma).

Chemical analyses of HH103 rkpA and rkpM LPS

Monosaccharides were identified as acetylated *O*-methyl glycoside derivatives obtained by methanolysis (1.25 M HCl/MeOH, 85 °C, 16 h) followed by acetylation with acetic anhydride in pyridine (80 °C, 30 min) (41). To define the sugar linkage pattern, including uronic acids and Kdo, an aliquot of each sample was methylated with iodomethane, treated with sodium tetradeuteroborate ($NaBD_4$) to transform the methyl ester functions of acidic sugars in a hydroxymethyl group with two deuterium atoms, and then hydrolyzed with TFA (2 M, 100 °C, 2 h), carbonyl-reduced by employment again of $NaBD_4$, acetylated with acetic anhydride and pyridine, and analyzed by gas LC-MS (GLC-MS) (41, 50). The absolute configuration of sugar residues has been determined by GLC-MS analysis of the acetylated *O*-(+)-2-octyl glycoside derivatives and comparison with authentic standards (41, 51).

The total fatty acid content was established by treating each LPS with 4 M HCl (100 °C, 4 h) and followed by a treatment with 5 M NaOH (100 °C, 30 min). The pH was adjusted to reach slight acidity. Fatty acids, after extraction in $CHCl_3$, were methylated with diazomethane and analyzed by GLC-MS. The ester-bound fatty acids were selectively released by base-catalyzed hydrolysis with aqueous 0.5 M NaOH, MeOH (1:1, v/v, 85 °C, 2 h), and then the product was acidified, extracted in chloroform, methylated with diazomethane, and analyzed by GLC-MS. Moreover, an aliquot of each LPS fraction (0.5 mg) was also methanolized with 1.25 M HCl/CH_3OH (80 °C for 16 h). The mixture underwent three extractions with hexane. The hexane layer, containing the fatty acids as methyl ester derivatives, was then analyzed by GLC-MS.

All the above derivatives were analyzed on Agilent Technologies gas chromatograph 6850A interfaced with mass spectrometry and a selective mass detector 5973N equipped with a SPB-5 capillary column (Supelco, 30 m by 0.25 mm inner diameter, flow rate of 0.8 ml min^{-1} using He as gas carrier). Electron impact mass spectra were recorded with an ionization energy of 70 eV and an ionizing current of 0.2 mA.

Isolation of the lipid A and the oligosaccharides $OS1_{rkpA}$ and $OS1_{rkpM}$

The **OS1** fractions of the two HH103 mutants investigated were obtained by mild acid hydrolysis. Purified LPS (~10 mg) was dissolved in acetate buffer (1 ml, pH 4.4). SDS (1 mg ml^{-1}) was added and hydrolysis proceeded (100 °C, 2 h). The solutions were extracted three times with $CHCl_3$/MeOH/H_2O (100:100:30, v/v/v) and centrifuged (4 °C, 8,800 × *g*, 20 min). The organic phases containing the lipid A moiety were further purified by several washes with distilled water, lyophilized, and then analyzed by MALDI-TOF MS. The water phases, containing the **OS1** fractions, were recovered and lyophilized. These **OS1** fractions were then purified by gel filtration chromatography on a Bio-Gel P-4 column (Bio-Rad, 1.5 by 100 cm, eluent of distilled water) and then, once dissolved in 50 mM NH_4HCO_3, further purified via HPLC by using a TSKgel G5000PWXL column (Supelco-Sigma, run in 50 mM NH_4HCO_3 at 0.8 ml min^{-1}, mounted on an Agilent 1100 system equipped with a refractive index and a UV detector, this last set at 206 nm).

Isolation of the oligosaccharides $OS2_{rkpA}$ and $OS2_{rkpM}$

To remove *O*-linked acyl chains, an aliquot of each sample was treated with anhydrous hydrazine, stirred at 37 °C for 60 min, cooled, poured into ice-cold acetone, and allowed to precipitate. The precipitate was centrifuged (1,200 × *g*, 30 min), washed with cold acetone in an ice bath, dried, dissolved in water, and lyophilized (52). The *O*-deacylated product was then *N*-deacylated with KOH (4 M, 120 °C, 16 h). After adjustment of the pH, free fatty acids were removed by several extractions with $CHCl_3$ followed by centrifugation (1,200 × *g*, 30 min). The aqueous phase of each sample was then lyophilized, and the produced salts were removed by size-exclusion chromatography on a Sephadex G-10 column (Pharmacia, 50 by 1.5 cm, eluent of distilled water) to yield **$OS2_{rkpA}$** and **$OS2_{rkpM}$** fractions.

NMR spectroscopy of the isolated OS1 and OS2

1D and 2D ^{1}H NMR spectra were recorded on a Bruker 600 DRX equipped with a cryoprobe. The solvent employed was D_2O, the temperature was 298 K, and pD was 7. To obtain information on the NH chemical shifts, the experiments were

recorded in an H_2O-D_2O mixture (53). Spectra calibration was performed with internal acetone (δ_H 2.225 ppm, δ_C 31.45 ppm). The double-quantum filtered phase-sensitive correlation spectroscopy (DQF-COSY) experiment was carried out by using data sets of 4096 × 256 points. Total correlation spectroscopy (TOCSY) experiments were executed with spinlock times of 100 ms, using data sets (t1 × t2) of 4096 × 256 points. Rotating frame Overhauser enhancement spectroscopy (ROESY) and NOESY experiments were recorded by using data sets (t1 × t2) of 4096 × 256 points and by using mixing times between 100 and 400 ms. In all homonuclear experiments, the data matrix was zero-filled in both dimensions to give a matrix of 4 K × 2 K points and was resolution enhanced in both dimensions by a cosine-bell function before Fourier transformation. The determination of coupling constants was obtained by 2D phase-sensitive DQF-COSY (54, 55). Heteronuclear single quantum coherence (^{1}H-^{13}C HSQC) and heteronuclear multiple bound correlation (^{1}H-^{13}C HMBC) experiments were recorded in ^{1}H-detection mode by single-quantum coherence with proton decoupling in the ^{13}C domain using data sets of 2048 × 256 points. ^{1}H-^{13}C HSQC was executed using sensitivity improvement and in the phase-sensitive mode using Echo/Antiecho gradient selection, with multiplicity editing during the selection step (56). The ^{1}H-^{13}C HMBC experiment was optimized on long-range coupling constants with a low-pass *J* filter to suppress one-bound connectivity, using gradient pulses for selection. A delay of 60 ms was employed for the evolution of long-range correlations. It was used a long-range coupling constant value of 6 Hz. The data matrix in both heteronuclear experiments was extended to 2048 × 1024 points using forward linear prediction (57).

MALDI-TOF MS of intact LPS from HH103 rkpA and rkpM and their isolated lipid A fractions

MALDI-TOF mass spectra of intact LPS from HH103 *rkpA* were recorded in linear mode and negative ion polarity on an Applied Biosystems MDS SCIEX 4800 MALDI TOF/TOF™ analyzer, equipped with delayed extraction technology. Ions formed by a pulsed UV laser (Nd:YAG laser, λ = 355 nm) were accelerated by 24 kV. The MS structural investigation of HH103 *rkpM* LPS was performed in reflectron mode and negative ion polarity on an ABSCIEX TOF/TOF™ 5800 Applied Biosystems mass spectrometer equipped with an Nd:YAG laser (λ = 349 nm), with a 3-ns pulse width and a repetition rate of up to 1000 Hz. In both cases, LPS MALDI preparations were executed as previously reported (50, 58, 59). Reflectron MALDI-TOF MS spectra of lipid A isolated from both HH103 mutant strains analyzed in this work were recorded on the above-described AB SCIEX TOF/TOF™ 5800 Applied Biosystems mass spectrometer. Lipid A fractions were dissolved in $CHCl_3$/CH_3OH (50:50, v/v). The matrix solution was 2,4,6-trihydroxyacetophenone in CH_3OH/0.1% TFA/CH_3CN (7:2:1, v/v) at a concentration of 75 mg ml^{-1} (60). 0.5 μl of the sample and 0.5 μl of the matrix solution were deposited on a stainless steel plate and left to dry at room temperature.

Molecular and microbiological techniques

Bacterial strains and plasmids used in this work are listed in Table S6. *S. fredii* strains were grown at 28 °C on complete TY medium (61), liquid YMB (62), or liquid MM (63). YMA medium corresponds to YMB solidified with agar (20 g/liter). When necessary, the media were supplemented with antibiotics (concentrations in μg ml^{-1}): rifampicin (Rif), 25; tetracycline (Tc), 2–4 (10 for *Escherichia coli*); gentamycin (Gm), 5 (10 for *E. coli*); spectinomycin (Spc), 50 or 100.

Assays to determine bacterial tolerance to SDS were carried out in MM containing 0.35 or 0.52 mM SDS. A 50 mM SDS stock solution in water was sterilized by filtration (0.2-μm pore size) and added to sterile MM to reach final concentrations of 0.35 or 0.52 mM SDS. Aliquots (50 μl) of 10-fold dilutions of early-stationary bacterial cultures (OD_{600} of 1.0) were used to inoculate tubes containing 5 ml of MM supplemented with the detergent. Bacterial growth was spectrophotometrically monitored at 1, 2, and 5 days after inoculation. Similarly, assays to determine salt tolerance were carried out in MM supplemented with 100 or 150 mM NaCl.

PCR amplifications were carried out as previously described (64). Primers for PCR amplifications are listed in Table S4.

Nodulation tests

Plant tests were carried out on *Glycyrrhiza uralensis* (L), *Macroptilium atropurpureum* (Moc. & Sessé ex DC) Urb., and *Cajanus cajan* (L.) Millsp. Inoculated *G. uralensis* nodules were used as a source of bacteroids for the visualization of LPS electrophoretic profiles. *M. atropurpureum* and *C. cajan* plants were used for standard nodulation assays in which parameters of symbiotic significance were determined. Nodule structures by optic and electronic microscopy of nodules induced by the HH103 *rkpM* mutant were also investigated.

M. atropurpureum and *G. uralensis* seeds were surface sterilized by sequential exposure to sulfuric acid for 20 min and sodium hypochlorite 12% (w/s) for 5 min, followed by five washing steps with sterile distilled water. *C. cajan* seeds were sterilized by sequential exposure to 96% (v/v) ethanol for 30 s and sodium hypochlorite 12% (w/s) for 5 min.

Two germinated seeds of *G. uralensis* or *C. cajan* were transferred to individual Leonard jars containing 800 ml of sterilized vermiculite supplemented with Fåhraeus nutrient solution (64). Three *M. atropurpureum* germinated seeds were placed in 250-ml Leonard jars. Each seedling was inoculated with 1 ml of a particular bacterial culture grown in YMB (OD_{600} of 0.4–0.5). Inoculated plants were grown for seven (*M. atropurpureum*) or eight (*C. cajan*) weeks with a 16-h photoperiod at 25 °C in the light and 18 °C in the dark. Nitrogenase activity of *M. atropurpureum* nodules was detected by acetylene reduction assays as described previously (65). Briefly, *M. atropurpureum* roots were cut off and placed in a 10-ml sealed test tube or a 250-ml sealed flask, respectively. The reaction was started with an air gas phase containing 10% acetylene. After incubating for 1 h, ethylene was measured with a gas chromatograph (5890A Hewlett Packard) using a Porapack Q column and nitrogen carrier gas at 80 °C. Plant tops were dried at 80 °C for 48 h and weighed.

Bacteria were isolated from surface-sterilized nodules as previously reported (38). Bacteria isolated (70 colonies) from 7 nodules induced for each strain on *M. atropurpureum* or *C. cajan* roots showed the expected antibiotic resistance markers: Rif^R for HH103, Rif^R Gm^R for HH103 *rkpM* and *rkpA* mutants, and Rif^R Gm^R Tc^R for HH103 *rkpM* C.

Microscopy of nodules

Optical microscopy studies were carried out as previously described (66). Briefly, *M. atropurpureum* plants were inoculated and grown for seven weeks in a plant growth chamber. Small fragments of *M. atropurpureum* nodules then were immediately fixed in 4% (v/v) glutaraldehyde in 0.1 M cacodylate buffer, pH 7.2, for 2 h at 4 °C after collection. Samples were washed several times in 0.1 M cacodylate buffer, pH 7.2, dehydrated in acetone at progressively higher concentrations, and embedded in Spurr resine (low-viscosity embedding kit, by Dr. Spurr). The semithin sections (1 μm) were obtained on a Leica EM UC7 ultramicrotome, stained with Toluidine blue, and viewed in an Olympus BX61 light microscope.

Extraction of bacteroid cells from nodules

Bacteroids from *G. uralensis* nodules were extracted as previously described (67). Nodules were surface sterilized for 1 min in 100% bleach and then washed three times in water. Nodules were crushed in MMS [40 mM 3-(4-morpholino)-propane sulfonic acid, 20 mM KOH, 2 mM $MgSO_4$, 0.3 M sucrose, pH 7.0] buffer, and the liquid containing bacteroids was removed with a pipette. Large particles were removed by passing through a 40-μm cell strainer cap (BD Falcon, BD Biosciences, San Jose, CA, USA). Samples were centrifuged once at 70 × *g* for 5 min and posteriorly twice at 2200 × *g* for 5 min to resuspend the resulting pellet fraction in MMS medium. LPS extraction from isolated bacteroids was carried out by following the same protocol as that used for the extraction of LPS from free-living cultures (38).

Data availability

All data described are contained within the manuscript.

Acknowledgments—We thank the Centro de Investigación, Tecnología e Innovación (CITIUS), of the University of Seville for light microscopy facilities.

Author contributions—F. D. L., I. S., A. S., S. A.-J., M.-R.-C., M. S. D., A. P., D. G., J.-E. R.-S., A. M., and J.-M. V. conceptualization; F. D. L., I. S., A. S., S. A.-J., M.-R.-C., M. S. D., A. P., D. G., J.-E. R.-S., A. M., and J.-M. V. formal analysis; F. D. L., I. S., A. S., S. A.-J., M.-R.-C., M. S. D., A. P., D. G., J.-E. R.-S., A. M., and J.-M. V. funding acquisition; F. D. L., I. S., A. S., C. A.-V., S. A.-J., M.-R.-C., M. S. D., A. P., D. G., J.-E. R.-S., and J.-M. V. investigation; F. D. L., I. S., A. S., S. A.-J., M.-R.-C., M. S. D., A. P., D. G., J.-E. R.-S., A. M., and J.-M. V. writing-original draft; F. D. L., I. S., A. S., S. A.-J., M.-R.-C., M. S. D., A. P., D. G., J.-E. R.-S., A. M., and J.-M. V. writing-review and editing.

Funding and additional information—This work was funded by grants P11-CVI-7500 from the Andalusian Government, and BIO2016-78409-R from the Ministry of Economy and Competitiveness (Spanish Government). M. S. D. is a Career Member of CONICET and worked thanks to grant CONICET PIP 112-201501-00232.

Conflict of interest—The authors declare that they have no conflicts of interest with the contents of this article.

Abbreviations—The abbreviations used are: KPS, K-antigen polysaccharide; RSP, rhizobial surface polysaccharides; EPS, exopolysaccharides; LPS, lipopolysaccharides; CG, cyclic glucans; OS, oligosaccharide; Pse5NAc7(3OHBu), 5-acetamido-3,5,7,9-tetradeoxy-7-(3-hydroxybutyramido)-l-glycero-l-manno-nonulosonic acid; DQF-COSY, double-quantum filtered phase-sensitive correlation spectroscopy; TOCSY, total correlation spectroscopy; ROESY, rotating frame Overhauser enhancement spectroscopy; ^1H-^{13}C HSQC, heteronuclear single quantum coherence; ^1H-^{13}C HMBC, heteronuclear multiple bound correlation; NAc N-acetyl groups; VLCFA, very-long-chain fatty acids; OD_{600}, optical density at 600 nm; GLC-MS, gas LC-MS.

References

1. López-Baena, F. J., Ruiz-Sainz, J. E., Rodríguez-Carvajal, M. A., and Vinardell, J. M. (2016) Bacterial molecular signals in the *Sinorhizobium fredii*-soybean symbiosis. *Int. J. Mol. Sci.* **17,** 755 CrossRef
2. Gage, D. J. (2004) Infection and invasion of roots by symbiotic, nitrogen fixing rhizobia during nodulation of temperate legumes. *Mol. Biol. Rev.* **68,** 280–300 CrossRef Medline
3. Jones, K. M., Kobayashi, H., Davies, B. W., Taga, M. E., and Walker, G. C. (2007) How rhizobial symbionts invade plants: the *Sinorhizobium-Medicago* model. *Nat. Rev. Microbiol.* **5,** 619–633 CrossRef Medline
4. Krol, E., and Becker, A. (2009) Surface polysaccharides as fitness factors of rhizospheric nitrogen-fixing bacteria. in *Bacterial Polysaccharides: Current Innovations and Future Trends*, (Ullrich M., ed), pp. 187–211, Caister Academic Press, London
5. Janczarek, M., Rachwaø, K., Marzec, A., Grzadziel, J., and Palusińska-Szysz, M. (2015) Signal molecules and cell-surface components involved in early stages of the legume–rhizobium interactions. *Appl. Soil Ecol.* **85,** 94–113 CrossRef
6. Kawaharada, Y., Kelly, S., Nielsen, M. W., Hjuler, C. T., Gysel, K., Muszyński, A., Carlson, R. W., Thygesen, M. B., Sandal, N., Asmussen, M. H., Vinther, M., Andersen, S. U., Krusell, L., Thirup, S., Jensen, K. J., *et al.* (2015) Receptor-mediated exopolysaccharide perception controls bacterial infection. *Nature* **523,** 308–312 CrossRef Medline
7. Kawaharada, Y., Nielsen, M. W., Kelly, S., James, E. K., Andersen, K. R., Rasmussen, S. R., Füchtbauer, W., Madsen, L. H., Heckmann, A. B., Radutoiu, S., and Stougaard, J. (2017) Differential regulation of the Epr3 receptor coordinates membrane-restricted rhizobial colonization of root nodule primordia. *Nat. Commun.* **8,** 14534 CrossRef Medline
8. Vinardell, J.-M., Acosta-Jurado, S., Zehner, S., Göttfert, M., Becker, A., Baena, I., Blom, J., Crespo-Rivas, J. C., Goesmann, A., Jaenicke, S., Krol, E., McIntosh, M., Margaret, I., Pérez-Montaño, F., Schneiker-Bekel, S., *et al.* (2015) The *Sinorhizobium fredii* HH103 genome: a comparative analysis with *S. fredii* strains differing in their symbiotic behaviour with soybean. *Mol. Plant Microbe Interact.* **28,** 811–824 CrossRef Medline
9. Margaret, I., Becker, A., Blom, J., Bonilla, I., Goesmann, A., Göttfert, M., Lloret, J., Mittard-Runte, V., Rückert, C., Ruiz-Sainz, J. E., Vinardell, J. M., and Weidner, S. (2011) Symbiotic properties and first analyses of the genomic sequence of the fast growing model strain *Sinorhizobium fredii* HH103 nodulating soybean. *J. Biotechnol.* **155,** 11–19 CrossRef Medline
10. Rodríguez-Navarro, D. N., Rodríguez-Carvajal, M. A., Acosta-Jurado, S., Soto, M. J., Margaret, I., Crespo-Rivas, J. C., Sanjuan, J., Temprano, F., Gil-Serrano, A., Ruiz-Sainz, J. E., and Vinardell, J. M. (2014) Structure and biological roles of *Sinorhizobium fredii* HH103 exopolysaccharide. *PLoS ONE* **9,** e115391 CrossRef Medline

11. Crespo-Rivas, J. C., Margaret, I., Hidalgo, A., Buendía-Clavería, A. M., Ollero, F. J., López-Baena, J., Murdoch, P., Rodríguez-Carvajal, M. A., Soria-Díaz, M. E., Reguera, M., Lloret, J., Sumpton, D. P., Mosely, J. A., Thomas-Oates, J. E., van Brussel, A. A. N., *et al.* (2009) *Sinorhizobium fredii* HH103 *cgs* mutants are unable to nodulate determinate- and indeterminate-nodule forming legumes and overproduce an altered EPS. *Mol. Plant Microbe Interact.* **22,** 575–588 CrossRef Medline
12. Gil-Serrano, A. M., Rodríguez-Carvajal, M. A., Tejero-Mateo, P., Espartero, J. L., Menéndez, M., Corzo, J., Ruiz-Sainz, J. E., and Buendía-Clavería, A. M. (1999) Structural determination of a 5-acetamido-3,5,7,9-tetradeoxy-7-(3-hydroxybutyramido)-L-*glycero*-L-*manno*-nonusolonic acid-containing homopolysaccharide isolated from *Sinorhizobium fredii* HH103. *Biochem. J.* **342,** 527–535 CrossRef
13. Chataigné, G., Couderc, F., and Poinsot, V. (2008) Polysaccharides analysis of sinorhizobial capside by on-line anion exchange chromatography with pulse amperiometric detection and mass spectrometry coupling. *J. Chromatogr. A* **1185,** 241–250 CrossRef Medline
14. Parada, M., Vinardell, J. M., Ollero, F. J., Hidalgo, A., Gutiérrez, R., Buendía Clavería, A., Lei, W., Margaret, I., López-Baena, F. J., Gil-Serrano, A., Rodríguez Carvajal, M. A., Moreno, J., and Ruiz-Sainz, J. E. (2006) *Sinorhizobium fredii* HH103 mutants affected in capsular polysaccharide (KPS) are impaired for nodulation with soybean and *Cajanus cajans*. *Mol. Plant Microbe Interact.* **19,** 43–52 CrossRef Medline
15. Hidalgo, A., Margaret, I., Crespo-Rivas, J. C., Parada, M., Murdoch, P. S., López, A., Buendía-Clavería, A. M., Moreno, J., Albareda, M., Gil-Serrano, A. M., Rodríguez-Carvajal, M. A., Palacios, J. M., Ruiz-Sainz, J. E., and Vinardell, J. M. (2010) The *rkpU* gene of *Sinorhizobium fredii* HH103 is required for bacterial K-antigen polysaccharide production and for efficient nodulation with soybean but not with cowpea. *Microbiology* **156,** 3398–3411 CrossRef Medline
16. Margaret-Oliver, I., Lei, W., Parada, M., Rodríguez-Carvajal, M. A., Crespo-Rivas, J. C., Hidalgo, Á., Gil-Serrano, A., Moreno, J., Rodríguez-Navarro, D. N., Buendía-Clavería, A., Ollero, J., Ruiz-Sainz, J. E., and Vinardell, J. M. (2012) *Sinorhizobium fredii* HH103 does not strictly require KPS and/or EPS to nodulate *Glycyrrhiza uralensis*, an indeterminate nodule-forming legume. *Arch. Microbiol.* **194,** 87–102 CrossRef Medline
17. Margaret, I., Crespo-Rivas, J. C., Acosta-Jurado, S., Buendía-Clavería, A. M., Cubo, M. T., Gil-Serrano, A., Moreno, J., Murdoch, P. S., Rodríguez-Carvajal, M. A., Rodríguez-Navarro, D. N., Ruiz-Sainz, J. E., Sanjuan, J., Soto, M. J., and Vinardell, J. M. (2012) *Sinorhizobium fredii* HH103 *rkp-3* genes are required for KPS biosynthesis, affect LPS structure and are essential for infection of legumes forming determinate nodules. *Mol. Plant Microbe Interact.* **25,** 825–838 CrossRef Medline
18. Di Lorenzo, F., De Castro, C., Lanzetta, R., Parrilli, M., Silipo, A., and Molinaro, A. (2015) Lipopolysaccharides as microbe-associated molecular patterns: a structural perspective. in *Carbohydrates in Drug Design and Discovery* (Jiménez-Barbero, J., Javier Canada, F., and Martín-Santamaría, S., eds.), pp. 38–63, Royal Society of Chemistry (RSC), London
19. Carlson, R. W., Forsberg, L. S., and Kannenberg, E. L. (2010) Lipopolysaccharides in *Rhizobium*-legume symbioses. in *Endotoxins: Structure, Function and Recognition*, (Wang X. and Quinn P. J., eds), pp. 339–386, Springer, New York
20. Silipo, A., Leone, M. R., Erbs, G., Lanzetta, R., Parrilli, M., Chang, W. S., Newman, M. A., and Molinaro, A. (2011) A unique bicyclic monosaccharide from the *Bradyrhizobium* lipopolysaccharide and its role in the molecular interaction with plants. *Angew. Chem. Int. Ed. Engl.* **50,** 12610–12612 CrossRef Medline
21. Silipo, A., Vitiello, G., Gully, D., Sturiale, L., Chaintreuil, C., Fardoux, J., Gargani, D., Lee, H. I., Kulkarni, G., Busset, N., Marchetti, R., Palmigiano, A., Moll, H., Engel, R., Lanzetta, R., *et al.* (2014) Covalently linked hopanoid-lipid A improves outer-membrane resistance of a *Bradyrhizobium* symbiont of legumes. *Nat. Commun.* **5,** 5106 CrossRef Medline
22. Di Lorenzo, F., Palmigiano, A., Duda, K. A., Pallach, M., Busset, N., Sturiale, L., Giraud, E., Garozzo, D., Molinaro, A., and Silipo, A. (2017) Structure of the lipopolysaccharide from the *Bradyrhizobium* sp. ORS285 *rfaL* mutant strain. *ChemistryOpen* **6,** 541–553 CrossRef Medline
23. Gudlavalleti, S. K., and Forsberg, L. S. (2003) Structural characterization of the lipid A component of *Sinorhizobium* sp. NGR234 rough and smooth form lipopolysaccharide. Demonstration that the distal amide-linked acyloxyacyl residue containing the long chain fatty acid is conserved in rhizobium and *Sinorhizobium* sp. *J. Biol. Chem.* **278,** 3957–3968 CrossRef
24. Brewin, N. J., Perotto, S., Kannenberg, E. L., Rae, A. L., Rathburn, E. A., Lucas, M. M., Kardailsky, I., Gunder, A., Bolaños, L., Donovan, N., and Drøbak, B. K. (1993) Mechanisms of cell and tissue invasion by *Rhizobium leguminosarum*: the role of cell surface interactions. in *Advances in Molecular Genetics of Plant-Microbe Interactions* (Nester E. W. and Verma D. P. S., eds.), pp. 369–380, Kluwer Academic Publishers, New York
25. Noel, K. D., van den Bosch, K. A., and Kulpaca, B. (1986) Mutation in *Rhizobium phaseoli* that lead to arrested development of infection threads. *J. Bacteriol.* **168,** 1392–1401 CrossRef Medline
26. Stacey, G., So, J. S., Roth, L. E., Lakshmi, B., and Carlson, R. W. (1991) A lipopolysaccharide mutant from *Bradyrhizobium japonicum* that uncouples plant from bacterial differentiation. *Mol. Plant Microbe Interact.* **4,** 332–340 CrossRef Medline
27. Lagares, A., Caetano-Anolles, G., Niehaus, K., Lorenzen, J., Ljunggren, H. D., Pühler, A., and Favelukes, G. (1992) A *Rhizobium meliloti* lipopolysaccharide mutant altered in competitiveness for nodulation of alfalfa. *J. Bacteriol.* **174,** 5941–5952 CrossRef Medline
28. Lagares, A., Hozbor, D. F., Niehaus, K., Otero, A. J., Lorenzen, J., Arnold, W., and Pühler, A. (2001) Genetic characterization of a *Sinorhizobium meliloti* chromosomal region in lipopolysaccharide biosynthesis. *J. Bacteriol.* **183,** 1248–1258 CrossRef Medline
29. Campbell, G. R., Reuhs, B. L., and Walker, G. C. (2002) Chronic intracellular infection of alfalfa nodules by *Sinorhizobium meliloti* requires correct lipopolysaccharide core. *Proc. Natl. Acad. Sci. U S A* **99,** 3938–3943 CrossRef Medline
30. Campbell, G. R., Sharypova, L. A., Scheidle, H., Jones, K. M., Niehaus, K., Becker, A., and Walker, G. C. (2003) Striking complexity of lipopolysaccharide defects in a collection of *Sinorhizobium meliloti* mutants. *J. Bacteriol.* **185,** 3853–3862 CrossRef Medline
31. Margaret, I., Lucas, M., Acosta-Jurado, S., Buendía-Clavería, A. M., Fedorova, E., Hidalgo, A., Rodríguez-Carvajal, M. A., Rodríguez-Navarro, D. N., Ruiz-Sainz, J. E., and Vinardell, J. M. (2013) The *Sinorhizobium fredii* HH103 lipopolysaccharide is not only relevant at early soybean nodulation stages but also for symbiosome stability in mature nodules. *PLoS ONE* **8,** e74717 CrossRef Medline
32. Carlson, R. W., Kalembasa, S., Turowski, D., Pachori, P., and Noel, K. D. (1987) Characterization of the lipopolysaccharide from a *Rhizobium phaseoli* mutant that is defective in infection thread development. *J. Bacteriol.* **169,** 4923–4928 CrossRef Medline
33. Cava, J. R., Elias, P. M., Turowski, D. A., and Noel, K. D. (1989) *Rhizobium leguminosarum* CFN42 genetic regions encoding lipopolysaccharide structures essential for complete nodule development on bean plants. *J. Bacteriol.* **171,** 8–15 CrossRef Medline
34. Noel, K. D., Forsberg, L. S., and Carlson, R. W. (2000) Varying the abundance of O-antigen in *Rhizobium etli* and its effect on symbiosis with *Phaseolus vulgaris*. *J. Bacteriol.* **182,** 5317–5324 CrossRef Medline
35. Gao, M., D'Haeze, W., De Rycke, R., Wolucka, B., and Holsters, M. (2001) Knockout of an azorhizobial dTDP-L-rhamnose synthase affects lipopolysaccharide and extracellular polysaccharide production and disables symbiosis with *Sesbania rostrata*. *Mol. Plant Microbe Interact.* **14,** 857–866 CrossRef Medline
36. Noh, J. G., Jeon, H. E., So, J. S., and Chang, W. S. (2015) Effects of the *Bradyrhizobium japonicum waaL* (*rfaL*) gene on hydrophobicity, motility, stress tolerance, and symbiotic relationship with soybeans. *Int. J. Mol. Sci.* **16,** 16778–16791 CrossRef Medline
37. Acosta-Jurado, S., Navarro-Gómez, P., Crespo-Rivas, J.-C., Medina, C., Murdoch, P. D. S., Cuesta-Berrio, L., Rodríguez-Carvajal, M.-Á., Ruiz-Sainz, J.-E., and Vinardell, J.-M. (2017) The *Sinorhizobium fredii* HH103 *rkp-2* region is involved in the biosynthesis of lipopolysaccharide and exopolysaccharide but not in K-antigen polysaccharide production. *Plant Soil* **417,** 415–431 CrossRef
38. Buendía-Clavería, A. M., Moussaid, A., Ollero, F. J., Vinardell, J. M., Torres, A., Moreno, J., Gil-Serrano, A. M., Rodríguez-Carvajal, M. A.,

Tejero-Mateo, P., Peart, J. L., Brewin, N. J., and Ruiz Sainz, J. E. (2003) A *purL* mutant of *Sinorhizobium fredii* HH103 is symbiotically defective and altered in its lipopolysaccharide. *Microbiology* **149,** 1807–1818 CrossRef Medline

39. Crespo-Rivas, J. C., Guefrachi, I., Mok, K. C., Villaécija-Aguilar, J. A., Acosta-Jurado, S., Pierre, O., Ruiz-Sainz, J. E., Taga, M. E., Mergaert, P., and Vinardell, J. M. (2016) *Sinorhizobium fredii* HH103 bacteroids are not terminally differentiated and show altered O-antigen in nodules of the inverted repeat-lacking clade legume *Glycyrrhiza uralensis*. *Environ. Microbiol.* **18,** 2392–2404 CrossRef Medline
40. Westphal, O., and Jann, K. (1965) Bacterial lipopolysaccharides extraction with phenol-water and further applications of the procedure. *Methods Carbohydr. Chem.* **5,** 83–91
41. De Castro, C., Parrilli, M., Holst, O., and Molinaro, A. (2010) Microbe-associated molecular patterns in innate immunity: extraction and chemical analysis of gram-negative bacterial lipopolysaccharides. *Methods Enzymol.* **480,** 89–115 CrossRef Medline
42. Knirel, Y. A., Shashkov, A. S., Tsvetkov, Y. E., Jansson, P. E., and Zähringer, U. (2003) Tetradeoxynon-2-ulosonic acids in bacterial glycopolymers: chemistry and biochemistry. *Adv. Carbohydr. Chem. Biochem.* **58,** 371–417 CrossRef
43. Dowdle, S. F., and Bohlool, B. B. (1985) Predominance of fast-growing *Rhizobium japonicum* in a soybean field in the People's Republic of China. *Appl. Environ. Microbiol.* **50,** 1171–1176 CrossRef
44. Thomas-Oates, J., Bereszczak, J., Edwards, E., Gill, A., Noreen, S., Zhou, J. C., Chen, M. Z., Miao, L. H., Xie, F. L., Yang, J. K., Zhou, Q., Yang, S. S., Li, X. H., Wang, L., Spaink, H. P., *et al.* (2003) A catalogue of molecular, physiological and symbiotic properties of soybean-nodulating rhizobial strains from different soybean cropping areas of China. *Syst. Appl. Microbiol.* **26,** 453–465 CrossRef Medline
45. Reuhs, B. L., Geller, D. P., Kim, J. S., Fox, J. E., Kolli, V. S. K., and Pueppke, S. G. (1998) *Sinorhizobium fredii* and *Sinorhizobium meliloti* produce structurally conserved lipopolysaccharides and strain-specific K antigens. *Appl. Environ. Microbiol.* **64,** 4930–4938 CrossRef Medline
46. Le Quéré, A. J. L., Deakin, W. K., Schmeisser, C., Carlson, R. W., Streit, W. R., Broughton, W. J., and Forsberg, L. S. (2006) Structural characterization of a K-antigen capsular polysaccharide essential for normal symbiotic infection in *Rhizobium* sp. NGR234. *J. Biol. Chem.* **281,** 28981–28992 CrossRef Medline
47. Kiss, E., Kereszt, A., Barta, F., Stephens, S., Reuhs, B. L., Kondorosi, A., and Putnoky, P. (2001) The *rkp-3* gene region of *Sinorhizobium meliloti* Rm41 contains strain-specific genes that determine K antigen structure. *Mol. Plant Microbe Interact.* **14,** 1395–1403 CrossRef Medline
48. Acosta-Jurado, S., Rodríguez-Navarro, D. N., Kawaharada, Y., Perea, J. F., Gil-Serrano, A., Jin, H., An, Q., Rodríguez-Carvajal, M. A., Andersen, S. U., Sandal, N., Stougaard, J., Vinardell, J. M., and Ruiz-Sainz, J. E. (2016) *Sinorhizobium fredii* HH103 invades *Lotus burttii* by crack entry in a Nod factor and surface polysaccharide-dependent manner. *Mol. Plant Microbe Interact.* **29,** 925–937 CrossRef Medline
49. Bourassa, D. V., Kannenberg, E. L., Sherrier, D. J., Buhr, R. J., and Carlson, R. W. (2017) The lipopolysaccharide lipid A long-chain fatty acid is important for the *Rhizobium leguminosarum* growth and stress adaptation in free-living and nodule environments. *Mol. Plant-Microbe Interact.* **30,** 161–175 CrossRef Medline
50. Di Lorenzo, F., Sturiale, L., Palmigiano, A., Lembo-Fazio, L., Paciello, I., Coutinho, C. P., Sá-Correia, I., Bernardini, M., Lanzetta, R., Garozzo, D., Silipo, A., and Molinaro, A. (2013) Chemistry and biology of the potent endotoxin from a *Burkholderia dolosa* clinical isolate from a cystic fibrosis patient. *Chembiochem* **14,** 1105–1115 CrossRef Medline
51. Leontein, K., Lindberg, B., and Lönngren, J. (1978) Assignment of absolute configuration of sugars by glc of their acetylated glycosides formed from chiral alcohols. *Methods Carbohydr. Chem.* **62,** 359–362 CrossRef
52. Holst, O. (2000) Deacylation of lipopolysaccharides and isolation of oligosaccharide phosphates. *Methods Mol. Biol.* **145,** 345–353 CrossRef Medline
53. Kasimova, A. A., Shneider, M. M., Arbatsky, N. P., Popova, A. V., Shashkov, A. S., Miroshnikov, K. A., Balaji, V., Biswas, I., and Knirel, Y. A. (2017) Structure and gene cluster of the K93 capsular polysaccharide of *Acinetobacter baumannii* B11911 containing 5-*N*-acetyl-7-*N*-[(*R*)-3-hydroxybutanoyl]pseudaminic acid. *Biochemistry* **82,** 483–489 CrossRef Medline
54. Piantini, U., Sorensen, O. W., and Ernst, R. R. (1982) Multiple quantum filters for elucidating NMR coupling networks. *J. Am. Chem. Soc.* **104,** 6800–6801 CrossRef
55. Rance, M., Sørensen, O. W., Bodenhausen, G., Wagner, G., Ernst, R. R., and Wüthrich, K. (2012) Improved spectral resolution in COSY (1)H NMR spectra of proteins via double quantum filtering. *Biophys. Res. Commun.* **425,** 527–533 CrossRef
56. States, D. J., Haberkorn, R. A., and Ruben, D. J. (1982) A two-dimensional nuclear Overhauser experiment with pure absorption phase in four quadrants. *J. Magnetic Res.* **48,** 286–292 CrossRef
57. Stern, A. S., Li, K. B., and Hoch, J. C. (2002) Modern spectrum analysis in multidimensional NMR spectroscopy: comparison of linear-prediction extrapolation and maximum-entropy reconstruction. *J. Am. Chem. Soc.* **124,** 1982–1993 CrossRef Medline
58. Sturiale, L., Palmigiano, A., Silipo, A., Knirel, Y. A., Anisimov, A. P., Lanzetta, R., Parrilli, M., Molinaro, A., and Garozzo, D. (2011) Reflectron MALDI TOF and MALDI TOF/TOF mass spectrometry reveal novel structural details of native lipooligosaccharides. *J. Mass Spectrom.* **46,** 1135–1142 CrossRef Medline
59. Sturiale, L., Garozzo, D., Silipo, A., Lanzetta, R., Parrilli, M., and Molinaro, A. (2005) New conditions for matrix-assisted laser desorption/ionization mass spectrometry of native bacterial R-type lipopolysaccharides. *Rapid Commun. Mass Spectrom.* **19,** 1829–1834 CrossRef Medline
60. Di Lorenzo, F., Palmigiano, A., Al Bitar-Nehme, S., Sturiale, L., Duda, K. A., Gully, D., Lanzetta, R., Giraud, E., Garozzo, D., Bernardini, M. L., Molinaro, A., and Silipo, A. (2017) The lipid A from *Rhodopseudomonas palustris* strain BisA53 LPS possesses a unique structure and low immunostimulant properties. *Chemistry* **23,** 3637–3647 CrossRef Medline
61. Beringer, J. E. (1974) R factor transfer in *Rhizobium leguminosarum*. *J. Gen. Microbiol.* **84,** 188–198 CrossRef Medline
62. Vincent, J. M. (ed) (1970) The modified Fåhraeus slide technique. in *Appendix III, A Manual for the Practical Study of Root Nodule Bacteria*, pp 144–145, Blackwell Scientific, New York
63. Robertsen, B. K., Aman, P., Darvill, A. G., McNeil, M., and Albersheim, P. (1981) The structure of acidic extracellular polysaccharides secreted by *Rhizobium leguminosarum* and *Rhizobium trifolii*. *Plant Physiol.* **67,** 389–400 CrossRef Medline
64. Vinardell, J. M., Ollero, F. J., Hidalgo, A., López-Baena, F. J., Medina, C., Ivanov-Vangelov, K., Parada, M., Madinabeitia, N., Espuny, M. R., Bellogín, R. A., Camacho, M., Rodríguez-Navarro, D. N., Soria-Díaz, M. E., Gil-Serrano, A. M., and Ruiz-Sainz, J. E. (2004) NolR regulates diverse symbiotic signals of *Sinorhizobium fredii* HH103. *Mol. Plant Microbe Interact.* **17,** 676–685 CrossRef Medline
65. Acosta-Jurado, S., Alias-Villegas, C., Navarro-Gómez, P., Zehner, S., Murdoch, P. D., Rodríguez-Carvajal, M. A., Soto, M. J., Ollero, F. J., Ruiz-Sainz, J. E., Göttfert, M., and Vinardell, J. M. (2016) The *Sinorhizobium fredii* HH103 MucR1 global regulator is connected with the *nod* regulon and is required for efficient symbiosis with *Lotus burttii* and *Glycine max* cv. Williams. *Mol. Plant Microbe Interact.* **29,** 700–712 CrossRef Medline
66. Acosta-Jurado, S., Alias-Villegas, C., Navarro-Gómez, P., Almozara, A., Rodríguez-Carvajal, M. A., Medina, C., and Vinardell, J. M. (2020) *Sinorhizobium fredii* HH103 *syrM* inactivation affects the expression of a large number of genes, impairs nodulation with soybean and extends the host-range to *Lotus japonicus*. *Environ. Microbiol.* **22,** 1104–1124 CrossRef Medline
67. Finan, T. M., McWhinnie, E., Driscoll, B., and Watson, R. J. (1991) Complex symbiotic phenotypes result from gluconeogenic mutations in *Rhizobium meliloti*. *Mol. Plant Microbe Interact.* **4,** 386–389 CrossRef
68. Keyser, H. H., Hu, T. S., Bohlool, B. B., and Weber, D. F. (1982) Fast growing rhizobia isolated from root nodules of soybean. *Science* **215,** 1631–1632 CrossRef Medline
69. Lamrabet, Y., Bellogín, R. A., Cubo, T., Espuny, M. R., Gil, A., Krishnan, H. B., Megias, M., Ollero, F. J., Pueppke, S., Ruiz-Sainz, J. E., Spaink, H. P., Tejero-Mateo, P., Thomas-Oates, J., and Vinardell, J. M. (1999) Mutation in GDP-fucose synthesis genes of *Sinorhizobium fredii* alters Nod factors

and significantly decreases competitiveness to nodulate soybeans. *Mol. Plant Microbe Interact.* **12,** 207–217 CrossRef Medline

70. Madinabeitia, N., Bellogín, R. A., Buendía-Clavería, A. M., Camacho, M., Cubo, T., Espuny, M. R., Gil-Serrano, A., de Lyra, M. C. C. P., Mousaid, A., Ollero, F. J., Soria Díaz, M. E., Vinardell, J. M., Zeng, J., and Ruiz-Sainz, J. E. (2002) *Sinorhizobium fredii* HH103 has a truncated *nolO* gene due to a −1 frameshift mutation that is conserved among other geographically distant *S. fredii* strains. *Mol. Plant Microbe Interact.* **15,** 150–159 CrossRef Medline
71. Trinick, M. J. (1980) Relationships amongst the fast-growing *Rhizobium* of *Lablab purpureus*, *Leucaena leucocephala*, *Mimosa* sp., *Acacia farnesiana*, and *Sesbania grandiflora* and their affinities with other *Rhizobium* groups. *J. Appl. Bacteriol.* **49,** 39–53 CrossRef
72. Casse, F., Boucher, C., Julliot, J. S., Michel, M., and Denarié, J. (1979) Identification and characterization of large plasmids in *Rhizobium meliloti* using agarose-gel electrophoresis. *J. Gen. Microbiol.* **113,** 229–242 CrossRef
73. Kereszt, A., Kiss, E., Reuhs, B. L., Carlson, R. W., Kondorosi, A., and Putnoky, P. (1998) Novel *rkp* gene clusters of *Sinorhizobium meliloti* involved in capsular polysaccharide production and invasion of the symbiotic nodule: the *rkpK* gene codes a UDP-glucose dehydrogenase. *J. Bacteriol.* **180,** 5426–5431 CrossRef
74. Perotto, S., Brewin, N. J., and Kannenberg, E. L. (1994) Cytological evidence for a host defense response that reduces cell and tissue invasion in pea nodules by lipopolysaccharide-defective mutants of *Rhizobium leguminosarum* strain 3841. *Mol. Plant Microbe Interact.* **7,** 99–112 CrossRef